1986A&A...168..311S

Astron. Astrophys. 168, 311–329 (1986)

ASTRONOMY
AND
ASTROPHYSICS

Velocities in solar magnetic fluxtubes

S.K. Solanki

Institute of Astronomy, ETH-Zentrum, CH-8092 Zürich Switzerland

Received March 19, accepted May 23, 1986

Summary. Stokes V zero-crossing wavelengths and the profiles of I_V (i.e. the integrated Stokes V profile, an approximation of Stokes I in magnetic fluxtubes), of a large number of unblended Fe I and II lines measured simultaneously with a Fourier transform spectrometer, are used to investigate the velocities in solar magnetic fluxtubes. The Stokes V zero-crossing wavelength shifts are determined both relative to the simultaneously observed Stokes I wavelengths and to laboratory values (after correcting for shifts introduced by solar-terrestrial relative motion, etc.). Within the accuracy of approximately $250\,\mathrm{m\,s^{-1}}$ of the absolute wavelength scale no net flows are seen in the photospheric layers of fluxtubes at disk centre, in both active region plages and the quiet network. The strong Mg Ib lines also show no shifts within the limit of the above accuracy. Neither do the Stokes V zero-crossing wavelength shifts relative to the wavelengths of the Stokes I profiles provide any support for the presence of the downflows inside fluxtubes which have been reported in a number of previous studies in the literature. However, the Stokes V shifts relative to Stokes I in the network are systematically different from such shifts in active region plages. This difference may be explained by a decrease in the granular blueshift of the Stokes I profile in active regions.

With the help of one-dimensional LTE model calculations it is shown that the observed line profiles (i.e. both line depth and width of a large number of lines) formed inside a fluxtube can only be reproduced if the model profiles are broadened by velocity. Estimates of the velocity amplitudes are derived by approximating the motions with macro- and microturbulence. The maximum rms value of the total turbulent velocity is found to be approximately $3.0 - 3.5\,\mathrm{km\,s^{-1}}$. The value of the empirically determined turbulence velocity is also studied as a function of the assumed fluxtube temperature structure and of the empirical damping factor. An upper limit of $1.5\,\mathrm{km\,s^{-1}}$ is set on the microturbulence. The dependence of the total turbulent velocity on line strength in the fluxtube is found to differ strongly from its dependence in the quiet photosphere, suggesting that the observed line broadening is not due simply to the photospheric velocities which may affect the magnetic signal via the expanding geometry of the fluxtube.

Finally, a strong correlation between the amplitude asymmetry of Stokes V and the magnitude of the macroturbulence is shown to exist, supporting the view that the asymmetry is closely related to velocity.

Key words: solar magnetic fields – fluxtubes – active regions – network – velocity – macroturbulence – microturbulence

1. Introduction

Despite the large amount of interest which small fluxtubes have attracted in recent years (for an overview see e.g. Stenflo, 1976; Harvey, 1977; Spruit and Roberts, 1983; Stenflo, 1985, and references therein), their structure and many of their basic properties remain uncertain. This is also true of the motions in their photospheric layers. Theoretically various kinds of motions in small fluxtubes have been extensively studied. Thus Unno and Ribes (1979), Schüssler (1984), and Hasan and Schüssler (1985) have studied the effects of steady flows on the properties and stability of fluxtubes. Hasan (1984, 1985) found that the convective collapse of fluxtubes gives rise to oscillatory motions within them. Finally, the wave modes possible in fluxtubes when the effects of gravity are included have been investigated by e.g. Defouw (1976), Roberts and Webb (1978, 1979), Spruit (1981), and Rae and Roberts (1982).

Observations of motions in the small fluxtubes, which make up a large fraction of all magnetic elements in the quiet network and in plages, are complicated by their small diameters, which generally lie below the best presently available spatial resolution. The spectrum observed in unpolarised light (Stokes I) is therefore contaminated by light coming from the non-magnetic surroundings of the fluxtubes, so that observations of Stokes V, the difference signal between right and left circularly polarised light, are required.

Early observational work with a spatial resolution of usually a couple of arc seconds, both in polarised and unpolarised light, suggested the presence of downflows of the order of $0.5\,\mathrm{km\,s^{-1}}$ co-spatial with the magnetic field, at supergranule boundaries (e.g. Frazier, 1970; Skumanich et al., 1975) and in active regions (e.g. Giovanelli and Ramsey, 1971; Howard, 1971). Giovanelli and Slaughter (1978) carried out an extensive empirical study of steady flows inside small fluxtubes by measuring the zero-crossing wavelength of the Stokes V profiles (relative to their Stokes I wavelengths) of a number of lines formed at different heights in the atmosphere, and so were able to determine the height variation of downflow velocity. They found that the velocity increases rapidly with depth, being negligible in the chromosphere and increasing to $1.6\,\mathrm{km\,s^{-1}}$ near the $\tau = 1$ level of the photosphere. Wiehr (1985) also finds redshifts of the V profile compared to Stokes I of between 0 and $2\,\mathrm{km\,s^{-1}}$ for the Fe I 8468.4 Å line in different magnetic elements.

Stenflo and Harvey (1985), on the other hand, observed only redshifts smaller than $0.3\,\mathrm{km\,s^{-1}}$ of the zero-crossing of the Stokes V profiles of the Fe I lines at 5250.2 Å and 5247.1 Å, with respect to the core wavelengths of the simultaneously obtained Stokes

© European Southern Observatory • Provided by the NASA Astrophysics Data System

1986A&A...168..311S

I profiles. If the wavelengths of the corresponding I profiles are corrected for the effects of convective motions according to Dravins et al. (1981), then they find that the V profiles are actually *blueshifted* by 0.0 to 0.3 km s^{-1} (the blueshift increases with the amount of magnetic flux), but they only use this correction to enhance their conclusion that downdrafts are small or absent inside the fluxtubes. There are therefore conflicting claims in the literature regarding the presence of downflows in fluxtubes. Furthermore, all previous observations determine the shifts of Stokes V relative to Stokes I, and there are still some problems left with the precise core wavelengths of Stokes I profiles in active regions. Kaisig and Schröter (1983) find that the cores of six Fe I lines formed in active regions are blueshifted compared to their wavelengths in purely non-magnetic regions by approximately 0.05 – 0.25 km s^{-1}. On the other hand Livingston's (1982) observations suggest that the active region profile of the Fe I 5250.6 Å line has a relative *core* blueshift of the order of 0.01 – 0.02 km s^{-1} (although at equal intensity the active region profile is always redshifted as compared to the quiet sun profile), while Cavallini et al. (1985) observe active region relative redshifts of the order of 0.05 – 0.2 km s^{-1} for 3 Fe I lines. Finally Miller et al. (1984) find that the line cores of three Fe I lines observed at supergranular boundaries lie within $\pm$0.02 km s^{-1} of the cores of these lines in the quiet photosphere. All these measurements are limited to a few medium strong Fe I lines. The wavelengths of Fe II lines and of most Fe I lines have not been studied at all in active regions. In the light of these uncertainties we shall determine Stokes V zero-crossing shifts for a large number of lines, both with respect to the simultaneously measured Stokes I core wavelengths, and to laboratory wavelengths.

There has also been some observational evidence for the presence of non-stationary motions in fluxtubes. Although Giovanelli et al. (1978) failed to detect oscillatory motions besides the five minute oscillations in time series of Stokes V zero-crossing wavelength shifts, this does not imply the absence of all other oscillatory motions in fluxtubes. Their spatial resolution of 2″.5 × 3″.5 means that they probably observed a number of fluxtubes simultaneously, and could therefore detect only those oscillations in which all the fluxtubes were oscillating in phase. Five minute oscillations with amplitudes ranging between 0.1 and 0.25 km s^{-1} were also observed by Wiehr (1985). In addition, he presented observations of large changes in Stokes V zero-crossing wavelength, amplitude, and asymmetry on a time scale of a few minutes, which appear to be independent of the five minute oscillations.

The presence of unresolved motions in fluxtubes was also hinted at by the discovery that Stokes V profiles from the network and from plages observed with high spectral resolution, are distinctly asymmetric, i.e. the areas and the amplitudes of their blue wings are different from those of their red wings (Stenflo et al., 1984). It was later found that these asymmetries vary considerably with line strength and with the excitation potential of the lower level (Solanki and Stenflo, 1984). Auer and Heasley (1978) showed convincingly that assuming LTE and a one-dimensional model, the area asymmetry of the Stokes V profile can only be explained by the presence of velocity gradients inside the fluxtubes.

If we drop one or both of these assumptions (LTE and one spatial dimension), other mechanisms become possible. If we allow for fluxtube expansion, then flows outside the fluxtube may serve to produce such asymmetries. Such flows have appeared, for example, in the theoretical calculations of Deinzer et al. (1984). The presence of non-LTE effects has also been invoked to explain Stokes V asymmetries by Kemp et al. (1984) and Landi Degl'Innocenti (1985). However, even then it may not be possible to obtain large asymmetries completely without the presence of velocities (Landi Degl'Innocenti, 1985). In Sect. 4.5 we present some empirical evidence for a coupling between velocity broadening and the asymmetry of Stokes V profiles. Asymmetries may therefore contain detailed information on the structure of the velocity field in and around fluxtubes, but due to the lack of proper diagnostic methods this information can at present not be extracted easily.

Besides the zero-crossing wavelength and the asymmetry of Stokes V there is yet another indicator of velocities in fluxtubes. If the Stokes V profile is integrated to obtain the I_V profile (an approximation of the intensity profile of the line formed solely inside the fluxtube; cf. Sect. 2.3 and Solanki and Stenflo, 1984), then the difference in widths between the I_V profile and the observed Stokes I profile (the latter mostly containing information on the non-magnetic surroundings of the fluxtubes) is another measure of the velocity structure in the fluxtube, if the differences in temperature, pressure and magnetic field strength between the fluxtube and its surroundings are taken into account. Thus Solanki and Stenflo (1984) found that the observed I_V profiles of medium strong Fe I lines are much broader than profiles calculated using static fluxtube models.

In the present paper we shall try to obtain some information on the velocity amplitudes inside fluxtubes by modelling the widths of the I_V profiles of Fe I and II lines using macro- and microturbulence. We shall for the most part use the statistical approach outlined by Solanki and Stenflo (1984, 1985). This has the advantage of allowing a large number of lines formed at different heights and with different sensitivities to temperature and velocity to be used. However, to remove any doubts on the validity of this approach, model calculations of the complete profiles of a smaller sample of lines shall also be compared with the observations.

2. Observations and reduction

2.1. Observational data and selected lines

The observations were carried out on April 29 and 30, 1979 at Kitt Peak, with the McMath solar telescope and the one meter Fourier transform spectrometer (FTS) used as a polarimeter to record both *Stokes I* and *V* simultaneously. Spectra of five regions of varying magnetic flux were obtained near disk centre. The spectral range of each scan is approximately 1000 Å, and the spectral resolution lies between 360 000 and 500 000. The spatial resolution is determined by the circular entrance aperture of 10″ diameter, and the temporal resolution varies between approximately 20 minutes and 1 hour. Further details regarding the data are to be found in Stenflo et al. (1984). In addition, an FTS Stokes I spectrum of a quiet region near disk centre, recorded on April 29, 1979, is used as a reference in part of this work. In this way spurious effects arising from the large filling factors in active regions can be eliminated.

The Fe I and Fe II lines used are taken from the lists of unblended lines published by Stenflo and Lindegren (1977), and Dravins and Larsson (1984), respectively. Not all the published lines can be used for the analysis, however. The lines found to be blended or affected by noise by Solanki and Stenflo (1984,

© European Southern Observatory • Provided by the NASA Astrophysics Data System

1986A&A...168..311S

1985) have been dropped. For part of the analysis the laboratory wavelengths of the lines are required and only those lines for which such wavelengths are known to sufficient accuracy can be used. For the Fe I lines these are taken from Stenflo and Lindegren (1977), who either used the wavelengths listed by Crosswhite (1975), or calculated them from the energy levels where no wavelength measurements existed. The Fe II laboratory wavelengths are taken from Dravins and Larsson (1984) and Dravins et al. (1986), who list wavelengths determined by Johansson (1978). For some of the Fe II lines insufficient atomic data are available and these have not been included in the analysis. Following Dravins et al. (1981) we have also dropped a number of lines for which the difference between the laboratory and quiet sun wavelengths (taken from Pierce and Breckinridge, 1973) is exceptionally large. The laboratory wavelengths of the Mg Ib lines used in part of the analysis are taken from Moore (1972).

2.2. *Absolute wavelengths*

The determination of absolute zero-crossing wavelengths requires that the measured wavelengths be corrected for any error in calibration of the wavelength scale, for gravitational redshifts, and for the relative motion between the observer and the observed region.

The instrumental wavelength scale has been, whenever possible, checked by comparing the wavelengths of atmospheric lines taken from Pierce and Breckinridge (1973) with the wavelengths of these lines in our spectra. For two spectra it is possible to use the telluric O_2 lines between 6278 Å and 6307 Å. Of these, the lines found to be unblended by Balthasar et al. (1982) have been chosen. According to these authors the wavelengths of these lines should be stable to within $15\,\mathrm{m\,s^{-1}}$. Caccin et al. (1985), on the other hand, warn that pressure induced shifts and asymmetries of O_2 lines make them of questionable use as absolute wavelength standards. For two other spectra the 5420 Å and 5422.9 Å lines of H_2O are used, in the absence of anything better. One spectrum contains no suitable atmospheric absorptions. However, according to Brault (1978) the FTS wavenumber scale should be accurate to $0.0001\,\mathrm{cm^{-1}}$, and indeed, the FTS wavelength scale is found to reproduce the telluric absorption lines to within $0.05\,\mathrm{km\,s^{-1}}$ in all the spectra in which these are present.

Next, the gravitational redshift of $0.636\,\mathrm{km\,s^{-1}}$ is subtracted from the wavelengths, and finally the relative motion between the observer and the observed region is compensated for. This motion may be thought of being composed of a number of components (Howard and Harvey, 1970), the most important of which near disk centre are due to the rotation of the earth around its own axis, its orbital motion around the sun, and solar rotation. The velocity due to the first two components is calculated using a code described by Balthasar (1984). The limiting factor for the accuracy of these calculations is probably the smearing of the order of $50\,\mathrm{m\,s^{-1}}$ introduced by the long integration times of the observations. Its main effect would be to broaden the lines slightly, but due to the asymmetry of Stokes V it may also cause a small shift of the zero-crossing wavelength, which will however be much smaller than $50\,\mathrm{m\,s^{-1}}$ (Solanki and Stenflo, 1986). The rotation rate of the solar magnetic features has been studied by e.g. Stenflo (1974). His values of the rotational velocity at different latitudes are used to compensate for solar rotation. The main uncertainty in the wavelength shift due to solar rotation is introduced by the imprecise knowledge of the position of the FTS entrance hole on the solar surface. As an additional check on solar rotation the Stokes I core wavelength of a strong line, whose core is formed above the layer of granular motion and should therefore be unaffected by it, e.g. Mg I 5172.7 Å, is determined and compared to laboratory wavelengths. The difference between its solar and laboratory wavelength is $638\,\mathrm{m\,s^{-1}}$ which compares very well with the gravitational redshift of $636\,\mathrm{m\,s^{-1}}$, which is the only expected shift if granular influences are absent. This method has been outlined by Livingston (1983). However, the relatively broad core of this line limits the accuracy of the measurement of its core wavelength.

The total uncertainty, in the Stokes V zero-crossing shifts relative to the laboratory wavelengths, resulting from all the different sources, is estimated to be about $\pm 0.25\,\mathrm{km\,s^{-1}}$ for the four data files which contain telluric lines.

2.3. *The I_V profile and line parameters*

Part of our analysis requires that a line width be unambiguously defined for lines formed inside the fluxtube. Since the I profile of light coming from the fluxtubes alone cannot be measured directly with the spatial resolution available today, we have to derive the line width from the measured Stokes V profiles. A natural way to do this is to follow Solanki and Stenflo (1984, 1985) and calculate I_V out of the observed Stokes V profile:

$$\frac{I_C - I_V(\lambda)}{I_C} = -\frac{1}{\Delta\lambda_H}\int_{\lambda_1}^{\lambda}\frac{w(\lambda')V(\lambda')}{I_C}\,d\lambda' \qquad (1)$$

where $\Delta\lambda_H = 4.67\cdot10^{-13}\,g_{\mathrm{eff}}\lambda_V^2\langle B\rangle$ is the Zeeman splitting, with g_{eff} being the effective Landé factor of the line, λ_V its wavelength in Å, and $\langle B\rangle$ the average field strength in G. λ_1 is a wavelength lying sufficiently far in the wing, so that $V(\lambda_1)\approx 0$. In practice the choice of λ_1 is usually determined by noise and the proximity of neighbouring lines. I_c is the intensity of the continuum, and $w(\lambda)$ is a weighting function required to make the continuum on the red and blue sides of the I_V profile lie at the same level. The difference in continuum level is a result of the area asymmetry of the observed Stokes V profiles. If the detailed mechanism by which this asymmetry is produced were known, the asymmetry at each wavelength could be exactly compensated for by choosing an appropriate $w(\lambda)$. Since this is not the case, we have chosen $w(\lambda)$ such that it is constant for all $\lambda < \lambda_V$, jumps at λ_V to another value at which it remains for all $\lambda > \lambda_V$. Here λ_V is the zero-crossing wavelength in Å. This appears to us to be the simplest way of countering the effects of the area asymmetry and of ensuring that the continuum level is the same on both sides of the line. Detailed descriptions of these processes, as well as some remarks regarding the interpretation of I_V are to be found in Solanki and Stenflo (1984, 1985). We only repeat here that the I_V profile is a first order approximation of the Stokes I profile formed inside the fluxtube.

We wish to add, however, that the I_V profile has certain advantages over the Stokes V profile when low spatial resolution polarimeter data are compared with *one-dimensional* fluxtube models, as is the case in this work. Since our observations have low spatial resolution, the assumption that the magnetic flux in the field of view is the same at all heights in the photosphere is quite reasonable. For the model calculations we use the thin fluxtube approximation, which also conserves magnetic flux with height. However, the radiative transfer is carried out along only one ray (the axis of the fluxtube). This one-line-of-sight approxi-

© European Southern Observatory • Provided by the NASA Astrophysics Data System

1986A&A...168..311S

mation means that the magnetic flux as felt by the spectral lines, is not conserved with height. Due to the great sensitivity of the Stokes V amplitude on the amount of magnetic flux, synthetic Stokes V profiles of lines formed at different heights cannot be simultaneously compared with the respective observed profies, so that one of the main advantages of FTS data (the large number of observed lines) is lost. With the I_V profile this problem is greatly reduced, since the data can now be compared to calculated profiles of Stokes I which are considerably less sensitive to the amount of magnetic flux. However, other effects of the fluxtube geometry may still play an important role. This highlights the need for 1.5-D radiative transfer in conjunction with a 2-D fluxtube model; i.e. radiative transfer along more than one line of sight, where the emergent intensity of all the rays are added together to give a resultant profile which mimics a profile observed at low spatial resolution. An illustrative example is provided by van Ballegooijen (1985), who points out that the contribution functions and the emergent profiles of the Stokes parameters are quite different for different lines of sight in the fluxtube. However, at this stage of the study of fluxtube velocities we feel justified in using the simpler 1-D approach based on the I_V profile, which allows a much larger number of possible models to be calculated, due to its substantially smaller requirements on computional capacity.

Once the I_V profile has been calculated, it and Stokes I can easily be parameterised following Stenflo and Lindegren (1977) and Solanki and Stenflo (1984). Since the parameterisation has been described in detail in the above papers, we shall restrict ourselves to listing only those parameters which are of consequence for this work: Line depth (d_I and d_V; index I indicates that this symbol represents a parameter of Stokes I, index V that it represents a parameter of I_V), line strength (S_I and S_V), line width in velocity units (v_{D_I} and v_{D_V}; the line width is determined at four levels in the profile: $0.1d$, $0.3d$, $0.5d$, and $0.7d$ above the core intensity. If nothing is stated to the contrary, then the width at the half level, $0.5d$, is meant), laboratory wavelength of the line, $\lambda_{\rm lab}$, wavelength of the observed Stokes I line core, λ_I, and finally the wavelength of the I_V line core, λ_V (this is identical to the wavelength of the Stokes V zero-crossing, which is also denoted by the same symbol). We shall differentiate between the wavelength of Stokes V as derived directly from the spectra, λ_V, and the absolute wavelength, λ_V^*, obtained after correcting for the motion of the observer relative to the observed region.

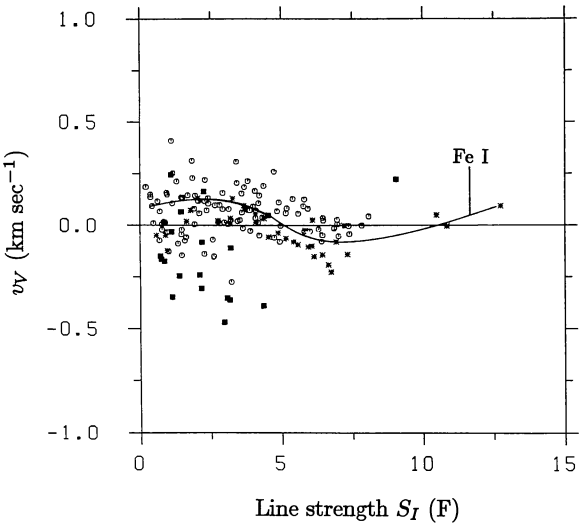

Fig. 1a. v_V vs. S_I, i.e. the difference in velocity units, between Stokes V zero-crossing absolute wavelength and the laboratory wavelength, vs. the line strength of the Stokes I profile. Plotted are the unblended Fe I and II lines in an FTS spectrum of an active region plage. In this and the following figures, the stars represent Fe I lines with $\chi_e < 3$ eV, the circles Fe I lines with $\chi_e \geq 3$ eV, and the filled squares Fe II lines. The solid curve is a smoothed mean curve of the Fe I data

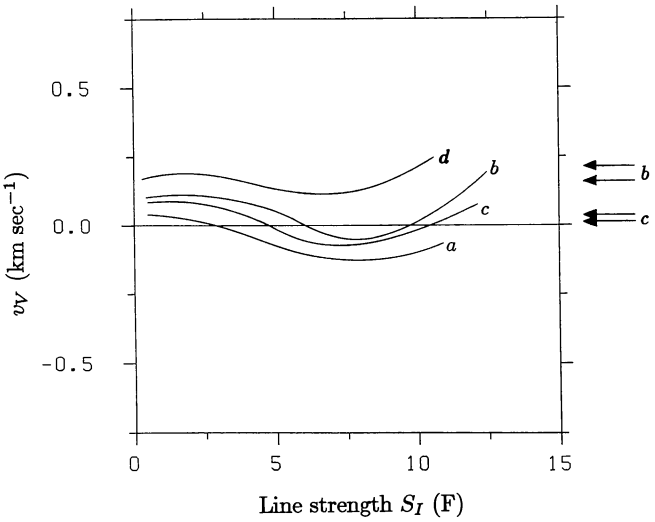

Fig. 1b. v_V vs. S_I for the smoothed mean curves of the Fe I lines formed in two active plages and in two network regions. The arrows denote the v_V values of the Mg Ib lines at 5172.7 Å and 5183.6 Å in two of the regions. The regions are denoted by the letters a, b (strong plage), and c, d (enhanced network). These letters mark the same regions in Figs. 1c, 3a, 3b, and 3c as well

3. Zero-crossing wavelengths

3.1. Analysis and results

In Fig. 1a the Stokes V zero-crossing shift relative to the laboratory wavelength, v_V, is plotted vs. S_I for a plage region. We define

$$v_V = c\frac{(\lambda_V^* - \lambda_{\rm lab})}{\lambda_{\rm lab}},$$

where c is the velocity of light, λ_V^* is the zero-crossing absolute wavelength of Stokes V, and $\lambda_{\rm lab}$ is the laboratory wavelength of the line. The stars represent Fe I lines with excitation potential of the lower level, $\chi_e < 3$ eV, the circles represent Fe I lines with $\chi_e \geq 3$ eV, and the filled squares Fe II lines. These symbols shall retain their meanings throughout the following figures. The scatter is mostly due to noise in the data and to inaccuracies in the laboratory wavelengths, but some is of solar origin (see below). In particular the larger scatter of the Fe II data, as compared to Fe I, is probably due to inconsistencies in the laboratory wavelengths of the ionised species, since a similar scatter has also been observed for Stokes I alone by Dravins et al. (1986) who first proposed this interpretation. The solid curve represents the smoothed mean of the Fe I data.

Figure 1b shows the smoothed mean v_V curves of the Fe I lines of four regions (marked a, b, c, and d in this and the

© European Southern Observatory • Provided by the NASA Astrophysics Data System

1986A&A...168..311S

following figures), again plotted vs. S_I. Due to the uncertainty in its position on the solar disk and the absence of telluric lines to serve as wavelength standards, the fifth observed region has not been included. Note that in three regions the mean curves are blueshifted for some values of S_I and redshifted for other values. If we interpret Stokes V zero-crossing shifts as steady flows, then both up- and downflows should be present at different heights in these regions! One of the regions appears to show a downflow of around $0.15 - 0.2\,\mathrm{km\,s^{-1}}$, but within the error margin given in Sect. 2.2 all the data are compatible with an *absence* of global up- or downflows in small magnetic fluxtubes, in contrast to the results of a number of previous studies (e.g. Giovanelli and Slaughter, 1978; Harvey, 1977; Wiehr, 1985).

The arrows on the right hand side of Fig. 1b mark the zero-crossing shifts of the Mg I b lines at 5172 Å and 5183 Å for the two spectra in which these lines are present (regions *b* and *c*). These lines have strengths of approximately 38 F and 47 F respectively, after correcting for the blends in their wings. They also give upper limits of approximately $250\,\mathrm{m\,s^{-1}}$ for any net flows inside fluxtubes. This increases our confidence in the absolute wavelength values determined. The fact that the strong Mg I b lines and the much weaker Fe I lines are equally unshifted is completely contrary to the results of Giovanelli and Slaughter (1978), who find increasing redshift with decreasing line strength. This contradiction cannot be accounted for by any mistake in our absolute wavelength determination, since it is based only on the *relative* shifts between different simultaneously observed lines.

It is of interest to note that the curves representing the four regions all have a similar shape. Again, this shape is not affected by the uncertainty of $0.25\,\mathrm{km\,s^{-1}}$ derived in Sect. 2.2, since that does not apply to the relative shifts between the lines of the same region. Medium strong lines are slightly blueshifted compared to weak and very strong lines. Surprisingly therefore, the lines with largest amplitude asymmetry (see Fig. 3 of Solanki and Stenflo, 1985) also have the largest blueshifts. However, the noise in the data is relatively large and we require further evidence before accepting such a dependence of Stokes V wavelength shifts on line strength. This additional evidence is provided by the regression analysis carried out below.

In order to see if the Stokes V wavelength shifts are also dependent on other quantities besides the line strength, we carried out a regression of the following form (for Fe I lines only):

$$v_V = x_1 + x_2 S_I + x_3 S_I^2 + x_4 \chi_e v_{D_I} + x_5 g_{\mathrm{eff}} \lambda_I^2 / v_{D_I} + x_6 \langle g_{\mathrm{eff}} \rangle \lambda_I^2 / v_{D_I} . \quad (2)$$

This simple regression equation is not meant to be unique or exhaustive, but is rather thought of as being the simplest one describing the dependence of v_V on the line strength, S_I, the excitation potential, χ_e, the effective Landé factor, g_{eff}, and the wavelength, with reasonable accuracy. $\langle g_{\mathrm{eff}} \rangle$ in Eq. (2) signifies the average Landé factor of the sampled lines. The effects of adding further terms were studied, but were too small to warrant their retention. Instead of λ_I, S_I and v_{D_I} the respective parameters of the I_V profile can also be used without changing the results substantially. Unlike the regressions carried out for line width and line depth by Solanki and Stenflo (1984, 1985), no unique form of the x_5 (Zeeman splitting) term is obvious here from theoretical considerations. Different forms of the x_5 and x_6 (wavelength) terms were therefore tried, but again the results were not changed noticeably.

Besides the expected dependence on S_I (with x_2 being negative and x_3 positive), we found only a slight dependence of v_V on g_{eff} (at the level of $1.5 - 2\sigma$, a marginal dependence on the wavelength, and a small but noticeable dependence on χ_e (at the level of $2 - 4\sigma$ for the different regions). An increase in redshift with increasing χ_e is observed. This is consistent with the shape of the v_V vs. S_I curve, since for equal line strength, lines with higher excitation potential are formed deeper in the atmosphere, and should have line shifts comparable to those of weaker low χ_e lines. This is an additional indication that the dependence of v_V on S_I is real, and is not some artifact of the instrument or the data reduction procedure. This trend of $v_V(\chi_e)$ does not continue to Fe II lines, and they have been left out, since their inclusion in the regression analysis would have necessitated a more complex form of Eq. (2) with more free parameters.

The regression decreases the scatter of the points in Fig. 1a only slightly. We therefore conclude that it is mostly due to noise in our data, and partly also due in inconsistencies and scatter in the laboratory wavelength measurements.

Figure 1c shows the least squares fits for v_V of the Fe II lines in the same four regions as in Fig. 1b. The letters *a*, *b*, *c*, and *d* refer to the same four regions as in Fig. 1b. The dashed curves are the least-squares fits for two regions containing the strong Fe II 4923.9 Å line ($S_I \approx 9.3$ F), when it is not included in the fitting procedure. A comparison of Fig. 1c to 1b suggests that the weaker Fe II lines are blueshifted compared to Fe I lines of equal strength thus reversing the trend of increasing redshifts with increasing χ_e shown by the Fe I lines. This result explains why Eq. (2) is insufficient to handle Fe I and II simultaneously.

Next let us look at the shifts of Stokes V relative to the Stokes I profiles measured simultaneously in the same region. Figure 2 shows

$$v_{VI} = c \frac{(\lambda_V - \lambda_I)}{\lambda_I}$$

for a network region, plotted against the Stokes I line depth, d_I. The scatter is again mostly due to noise, which now has contri-

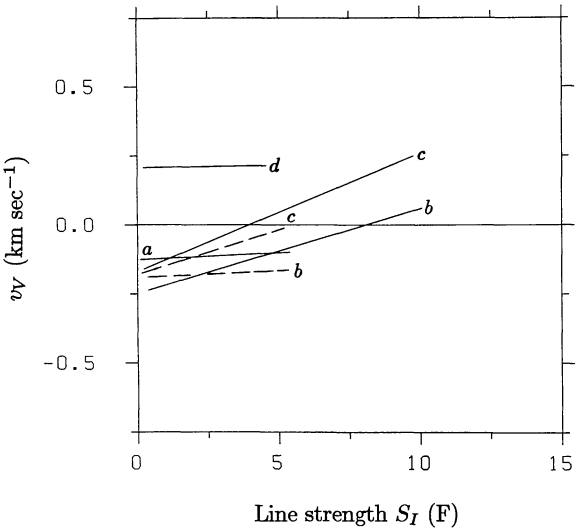

Fig. 1c. v_V vs. S_I for the least-squares fits to the Fe II data of four regions (solid lines). The dashed lines are the least-squares fits to the data of two regions containing the strong Fe II 4923.9 Å line, if it is neglected

© European Southern Observatory • Provided by the NASA Astrophysics Data System

1986A&A...168..311S

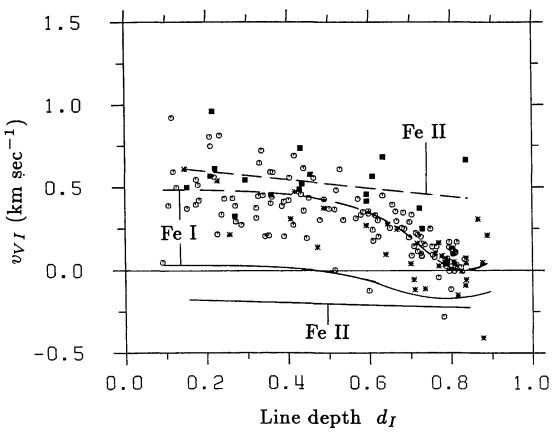

Fig. 2. v_{VI}, the difference, in velocity units, between Stokes V zero-crossing wavelength and the Stokes I core wavelength, vs. d_I, the line depth of Stokes I. The data are from an enhanced network region. The dashed curves denote the smoothed mean of the Fe I data, resp. a least-squares fit to the Fe II data (as marked in the figure). The solid curves are obtained from the dashed ones by removing the granular blueshift of the Stokes I profiles

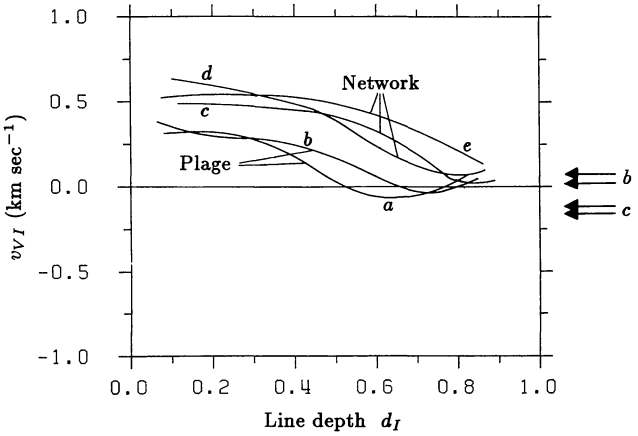

Fig. 3a. v_{VI} vs. d_I for the smoothed mean curves of the Fe I data of all five observed regions. The lower two curves are from strong active region plages (regions *a* and *b*), the upper three from enhanced network regions (*c*, *d*, and *e*). The arrows denote v_{VI} of the Mg Ib lines at 5172.7 Å and 5183.6 Å in two of the regions (*b* and *c*)

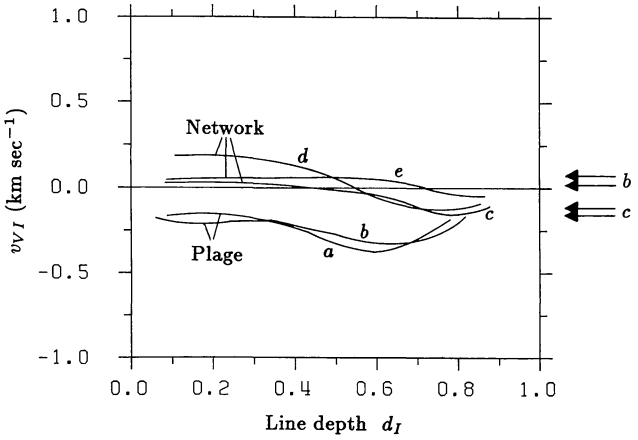

Fig. 3b. The same as in Fig. 3a, except that the granular blueshift of the Stokes I profiles has been removed using the quiet sun values of Dravins et al. (1981). The lower two curves again represent active regions

butions from the uncertainties in Stokes I as well as V wavelengths. The dashed curve represents the smoothed mean of the Fe I data. The dashed straight line is a least-squares fit to the Fe II data. The large relative redshift of the weak Stokes V lines is of course due to the increasing blueshift of the Stokes I profiles for decreasing line depth. Also shown are the 'corrected' smoothed mean curves for both Fe I and II (drawn solid). These are obtained from the original curves by subtracting the granular blueshifts of the Stokes I profiles from them. The values of the Fe I blueshifts have been taken from Dravins et al. (1981), the blueshifts of Fe II from Dravins and Larsson (1984). These authors list quiet sun mean blueshifts of groups of Fe I, resp. Fe II, lines having different line depths, wavelengths, and excitation potentials. The reason d_I was chosen as the abscissa instead of S_I is because the average Stokes I blueshifts given by Dravins et al. (1981) and Dravins and Larsson (1984) are ordered by line depth. The use of quiet sun values to compensate for Stokes I wavelength shifts in a network region needs to be justified. Miller et al. (1984) find that at supergranule boundaries the Stokes I wavelengths are very similar to those on the quiet sun. This is what one would expect if the filling factor, α, is small. In a simple two component model, α is defined as the fraction of the observed area covered by strong-field magnetic elements, the rest of the area being field free. For the network region plotted in Fig. 2 the filling factor is approximately 3% (Solanki and Stenflo, 1985), which is probably small enough for the Stokes I core wavelengths to remain largely unaffected by the magnetic field (cf. Miller et al. 1984). Finally, even if the quiet sun wavelengths may not be ideal for the task, the absence of any large body of such data from active regions makes them the only reasonable choice.

Figure 3a shows the *un*compensated mean Fe I v_{VI} curves of all five regions. Applying the quiet sun Stokes I blueshift compensations to these data results in the curves shown in Fig. 3b. The arrows on the right side of the figures mark v_{VI} of the Mg Ib lines at 5172 Å and 5183 Å. Since their Stokes I core wavelengths are expected to be practically unaffected by granular motions, no blueshift compensation has been carried out, and the arrows are at the same positions in Figs. 3a and b. A dependence of Stokes V wavelength shift (relative to Stokes I) on the filling factor is clearly evident, with the regions of small magnetic flux having Stokes V profiles showing practically no relative shifts at all, while the two plage regions show an average blueshift of approximately 250 m s^{-1}. This is in general agreement with what Stenflo and Harvey (1985) found for the Fe I 5250.2 Å line. We find no support for such a trend from the v_V curves in Fig. 1b (which is not too surprising, since its magnitude lies at the limit of the accuracy of the absolute wavelengths). A simple explanation for this behaviour of v_{VI} is that the Stokes V wavelengths remain unaffected by increasing filling factor, while the granular blueshift of the Stokes I profiles decreases progressively with increasing filling factor (perhaps due to magnetic suppression of convection near the fluxtubes), in accordance with the results of Cavallini et al. (1985) for three Fe I lines. This interpretation appears to be supported by Wiehr's (1985) observation that when scanning across a plage, the Stokes I profile is shifted, but the Stokes V wavelength remains unaffected. The use of the quiet sun Stokes

© European Southern Observatory • Provided by the NASA Astrophysics Data System

1986A&A...168..311S

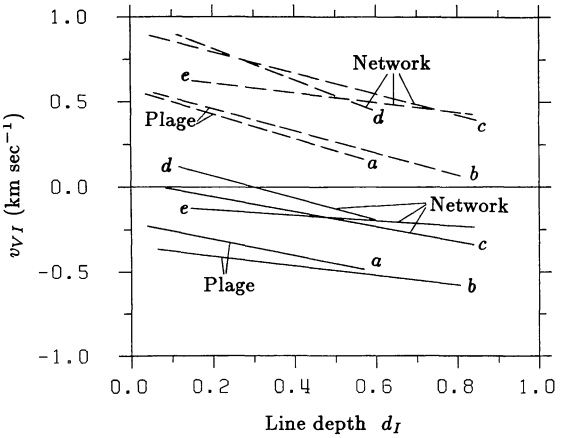

Fig. 3c. v_{VI} vs. d_I for the least-squares fits of the Fe II lines in the five observed regions. Dashed lines: original data. Solid lines: the data after compensating for the Stokes I blueshift

I blueshift values is therefore not justified for strong plages. However, the three regions with filling factor $\lesssim 5\%$ support the conclusion reached from the v_V data that only flows with small amplitudes are present in fluxtubes. They actually suggest an upper limit of about 200 m s^{-1} on the velocities of such flows.

Figure 3c shows the uncompensated (dashed) and compensated (solid) least-squares fits to the Fe II v_{VI} data. The average Fe II Stokes I granular blueshifts are considerably larger than the Fe I blueshifts according to Dravins and Larsson (1984) and Dravins et al. (1986), being of the order of 600–800 m s^{-1}. The two lowest curves in each group again belong to the two active region plages, suggesting that the granular blueshift of the Fe II Stokes I profiles, like that of the Fe I profiles, is reduced in active regions. The corrected v_{VI} values of Fe II lines again lie close to zero. They have a slight tendency to lie bluewards of the Fe I lines, confirming the trend suggested by the v_V data.

The comparison of the derived v_V and v_{VI} values also provides us with a method to check whether our data are grossly affected by the five minute oscillations, since v_V is susceptible to them, while v_{VI} is not (under the assumption that both Stokes I and V are shifted by approximately the same amount by them). From the similarity of the results of the analyses of v_V and v_{VI} (at least for the regions with low filling factor), we therefore conclude that the five minute oscillations do not significantly affect the results of this section, perhaps due to the relatively long integration times of our observations.

As the main result of this section we can set an upper limit on the Stokes V zero-crossing shifts of about ± 250 m s^{-1} in both network and active region plages. If such shifts are interpreted as being due to steady flows in magnetic fluxtubes, then the down- or upflow velocities have to be less than this value. Our data is therefore compatible with an absence of steady flows in small magnetic fluxtubes.

3.2. Comparison with transition zone velocities

Steady flows (i.e. flows having timescales of an hour or more) have been observed in the transition region over both quiet and active photosphere. For quiet regions at disk centre Gebbie et al. (1981) find spatially averaged RMS velocities of about ± 4 km s^{-1} in C IV. Above active regions the observed velocities are larger, being of the order of ± 5 to ± 10 km s^{-1} near disk centre in C IV (Athay et al., 1982). Both upward and downward flows have been observed, with downflows predominating. A correlation between photospheric magnetic field structure and transition region flow velocity also appears to exist. Over shorter timescales velocities with amplitudes of 15–20 km s^{-1} or even higher have been reported (Feldman et al., 1982; Dere et al., 1981). For the rest of this section we shall suppose that these flows are predominantly localised in magnetic structures having fluxtubes as their photospheric footpoints.

Assuming that the motions in active regions are mainly along magnetic field lines we can use the observed transition zone velocities to calculate the photospheric velocities in magnetic elements of a unipolar region from the conservation of mass. This requires a knowledge of the density in the transition region. Estimates of the electron density, n_e, in active regions have been made from O IV lines, which are formed at temperatures just slightly higher than C IV. However, depending on the method used quite different estimates of n_e are obtained, ranging from $n_e \approx (1-2)\,10^{10}$ cm^{-3} (Hayes, 1985) to $n_e \approx 8\,10^{10}$ cm^{-3} (Feldman and Doschek, 1978).

An upper limit for the velocity in the photosphere is obtained by using the higher values of the transition region velocities and electron densities. The total transition zone mass density, ρ, is then determined for $n(\mathrm{H})/n_e = 0.77$ (McWhirter et al., 1975). By taking the corresponding value of ρ in the photosphere from the HSRA (Gingerich et al., 1971) a value of less than 0.5 m s^{-1} is obtained for the steady flow velocity at the height of the temperature minimum ($\tau = 10^{-4}$).

So far the expansion of magnetic regions with height has not been taken into account. A limit can be set on this expansion by comparing the velocities measured in the active transition region and the upper bounds for photospheric fluxtube velocities derived in this paper. Thus one finds that the magnetic filling factor in the transition region can be up to 400 times larger than at the temperature minimum level for the parameters selected above. If the lower value of the transition zone density is assumed this upper limit will be correspondingly larger.

We therefore conclude that the limit set on the photosphere fluxtube flow velocity in this paper is easily compatible with both the large observed transition zone velocities and a dramatic chromospheric expansion of fluxtubes, the presence of which has been proposed on theoretical (e.g. Gabriel, 1976), as well as on observational grounds (e.g. Jones, 1985). However, at the present stage this is by no means a stringent limit and much greater accuracy in the measured photospheric line shifts is required if better limits on fluxtube expansion are to be set in this manner. A detailed comparison between transition-region and *chromospheric* velocities in active regions has been carried out by Mein et al. (1985).

4. Fluxtube velocity amplitudes derived from line broadening

In this section we shall analyse the I_V profile, whose width is determined by thermal Doppler broadening, radiative and collisional damping, Zeeman splitting, and mass motion induced Doppler broadening. Using simple representations of fluxtubes we shall model the profiles of Fe I and II lines and obtain a value for the rms velocity in fluxtubes by comparing them with observed I_V profiles.

© European Southern Observatory • Provided by the NASA Astrophysics Data System

1986A&A...168..311S

4.1. Fluxtube model and radiative transfer

The thin fluxtube approximation is used to describe the magnetic elements. This is a reasonable assumption, as was shown by Pneuman et al. (1986), who found only a small difference between the structures of fluxtubes calculated with and without magnetic tension, for tubes with diameters less than 200 km. In our model the temperature inside the fluxtube is first prescribed at all heights, the pressure is then calculated from the equation of hydrostatic equilibrium (here it is implicitly assumed that the velocities inside the fluxtubes or in their immediate surroundings are small compared to the sound speed, an assumption which is consistent with the subsequently obtained results; cf. Sect. 4.4). For a given Wilson depression (defined here as the depth at which the pressure inside the fluxtube equals the pressure at $\tau = 1$ outside) the magnetic field can be calculated as the square root of the pressure difference at a given height. The external atmosphere is represented by the HSRASP (Chapman, 1979), which is the HSRA (Gingerich et al., 1971) extended down into the convection zone by combining it with Spruit's (1974) convection zone model. The electron pressure and the opacity are calculated using the code of Gustafsson (1973).

The radiative transfer is handled using a modified version of the code described by Beckers (1969a, b). It assumes LTE and calculates all four Stokes parameters for any Zeeman splitting pattern in LS-coupling and for an arbitrary model atmosphere. Only one line of sight, along the fluxtube axis, is considered. Collisional damping is included, assuming Van der Waals interaction between the radiating atom and neutral hydrogen and helium in the generally used approximation given by Unsöld (1955). For our purposes this should be of sufficient accuracy. There are differing claims as far as the need for empirical corrections to the Van der Waals damping parameter, Γ_{Unsold}, are concerned. We have therefore carried out our calculations with two different values. a: With no empirical correction to the calculated damping parameters in the light of the results of Blackwell and Shallis (1979), i.e. $\delta_\Gamma = 1$, with δ_Γ being defined by $\Gamma_{\text{true}} = \delta_\Gamma \Gamma_{\text{Unsöld}}$. b: With a factor of 2.5 correction to $\Gamma_{\text{Unsöld}}$, as has been suggested by Holweger (1979), i.e. $\delta_\Gamma = 2.5$. The strongest lines in our sample have a non-negligible contribution from the atmosphere above the temperature minimum. To keep the chromospheric temperature rise from falsifying the LTE calculations, we have therefore changed the HSRASP temperature structure above the temperature minimum, so that $T(\tau)$ is parallel to that of the Holweger and Müller (1974) LTE solar atmosphere model. This gives reasonable quiet sun line profiles, even for the strongest lines considered, as will be shown in Sect. 4.2.

Two sets of thirty hypothetical Fe I and II line profiles, one each for $\delta_\Gamma = 1$ and 2.5, are calculated for each set of model parameters. These sets are divided into three groups, each containing 10 lines of different line strength. The first group is composed of Fe I lines with $\chi_e = 1.5$ eV, the second group of Fe I lines with $\chi_e = 4$ eV, and the third group of Fe II lines with $\chi_e = 3$ eV. After the radiative transfer calculations have been completed, the same line parameters are determined for the calculated Stokes I profiles as had previously been done for the observed I and I_V line profiles (see Sect. 2.3).

In addition to these hypothetical lines we also calculate the profiles of ten Fe I lines which have been carefully selected to fulfill different criteria that shall be described in detail in a later paper. The lines and some of their atomic and solar parameters are listed in Table 1. These lines serve to check how well the complete line profile is reproduced by the fitting of a small number of line parameters. An additional reason for fitting individual lines is to see how large the effects of non-zero Landé factors and anomalous Zeeman splitting are on the derived velocities (the hypothetical lines are all Zeeman triplets with $g = 0$).

4.2. Photospheric line profiles

In Sects. 4.3 and 4.4 we shall work with the differences and the ratios between the Stokes I and I_V profiles, since small differences between the properties of the fluxtubes and their surroundings show up much better in the profile differences and ratios than in I_V alone. This requires that the quiet sun profiles be modeled first, which also serves as a test for the codes and methods used. If we neglect its asymmetry, the mean photospheric Stokes I profile can be reproduced relatively well using a mixture of macro- and depth independent microturbulent broadening (e.g. Smith et al., 1976; Nordlund, 1978). For the microturbulence velocity a constant 0.8 km s^{-1} is chosen as suggested by Blackwell and Shallis (1979) for the HSRA. Following Smith et al. (1976) a macroturbulent velocity distribution having the shape of a Voigt function $H(a_{\text{mac}}, \xi_{\text{mac}})$ (a_{mac} is the ratio of 'damping' to 'Doppler' width and ξ_{mac} is the 'Doppler' width of the macroturbulent velocity profile, see

Table 1.

Ion	λ (Å)	Multiplet	Transition	χ_e (eV)	$g_{\text{eff}}^{\text{LS}}$	$g_{\text{eff}}^{\text{emp}}$	S_I (F)	ξ_{mac}^I (km s^{-1})	a_{mac}^I	ξ_{mac}^V (km s^{-1})
Fe I	5048.44	984	$z^3D_1^\circ - e^3D_2$	3.96	1.500	1.431	3.68	1.4	0.15	2.1
Fe I	5083.34	16	$a^5F_3 - z^5F_3^\circ$	0.96	1.250	1.250	6.63	1.2	0.12	3.3
Fe I	5127.68	1	$a^5D_3 - z^7D_2^\circ$	0.05	1.000	0.993	0.93	1.1	0.08	1.5
Fe II	5197.57	49	$a^4G_{2\frac{1}{2}} - z^4F_{1\frac{1}{2}}^\circ$	3.23	0.700	0.671	4.39	1.2	0.15	2.9
Fe I	5247.06	1	$a^5D_2 - z^7D_3^\circ$	0.09	2.000	1.992	3.53	1.3	0.10	1.9
Fe I	5250.22	1	$a^5D_0 - z^7D_1^\circ$	0.12	3.000	2.999	3.51	1.3	0.13	1.9
Fe I	5293.96	1031	$c^3F_3 - u^3D_2^\circ$	4.14	1.000	0.976	1.42	1.4	0.05	1.3
Fe I	5383.38	1146	$z^5G_5^\circ - e^5H_6$	4.31	1.083	1.123	8.12	1.1	0.20	3.3
Fe II	5414.07	48	$a^4G_{3\frac{1}{2}} - z^4D_{3\frac{1}{2}}^\circ$	3.22	1.206	1.190	1.40	1.8	0.07	2.0
Fe I	5445.05	1163	$z^3G_5^\circ - e^3G_5$	4.39	1.200	1.248	5.76	1.3	0.10	2.8

© European Southern Observatory • Provided by the NASA Astrophysics Data System

1986A&A...168..311S

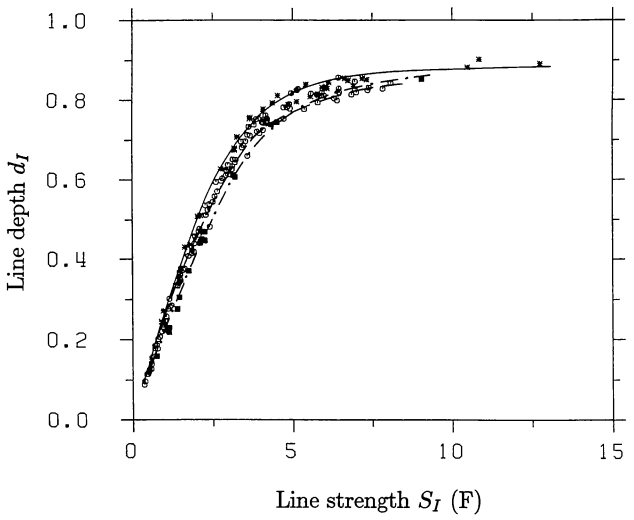

Fig. 4a. d_I vs. S_I for Fe I and II lines in the quiet photosphere. The symbols have the same meaning as in Fig. 1a. The three curves are model calculations. Solid curve: Fe I lines with $\chi_e = 1.5$ eV, dashed curve: Fe I lines with $\chi_e = 4$ eV, dot-dashed curve: Fe II lines with $\chi_e = 3$ eV. Empirical damping factor: $\delta_I = 2.5$

e.g. Mihalas, 1978) is then convoluted with the calculated line profile. The two free parameters per line are varied to give a best fit to the observed line parameters. Since, to our knowledge a similar analysis with such a large body of data has not been carried out previously, we illustrate the resulting fits in Figs. 4a and b for calculations with $\delta_I = 2.5$. In Fig. 4a the line depth, d_I, is plotted vs. line strength, S_I. The solid curve represents calculated Fe I lines with $\chi_e = 1.5$ eV, the dashed curve calculated Fe I lines with $\chi_e = 4$ eV, and the dot-dashed curve represents calculated Fe II lines. In Fig. 4b the line widths at the four chord levels $0.1d_I$, $0.3d_I$, $0.5d_I$, and $0.7d_I$ above line bottom are respectively plotted against S_I. A fit of comparable quality can be achieved with $\delta_I = 1$ as well, the only difference being that the derived macroturbulence velocities are somewhat different.

It will be noticed that the fit is not always perfect. For example, at the $0.1d_I$ chord only the Fe I data with $\chi_e \geq 3$ eV are well reproduced by the calculated profiles between $S_I = 5$ F and 10 F, the calculated Fe I, $\chi_e < 3$ eV and Fe II lines being too narrow. The strongest low exictation Fe I lines are not too well reproduced at all four chords either, departure from LTE probably being the main culprit. Figure 5 shows the parameters of the macroturbulence profile as a function of S_I. $\xi^I_{\rm mac}$, i.e. $\xi_{\rm mac}$ deduced from the Stokes I profile, is plotted in Fig. 5a, and $a^I_{\rm mac}$ in Fig. 5b. It should

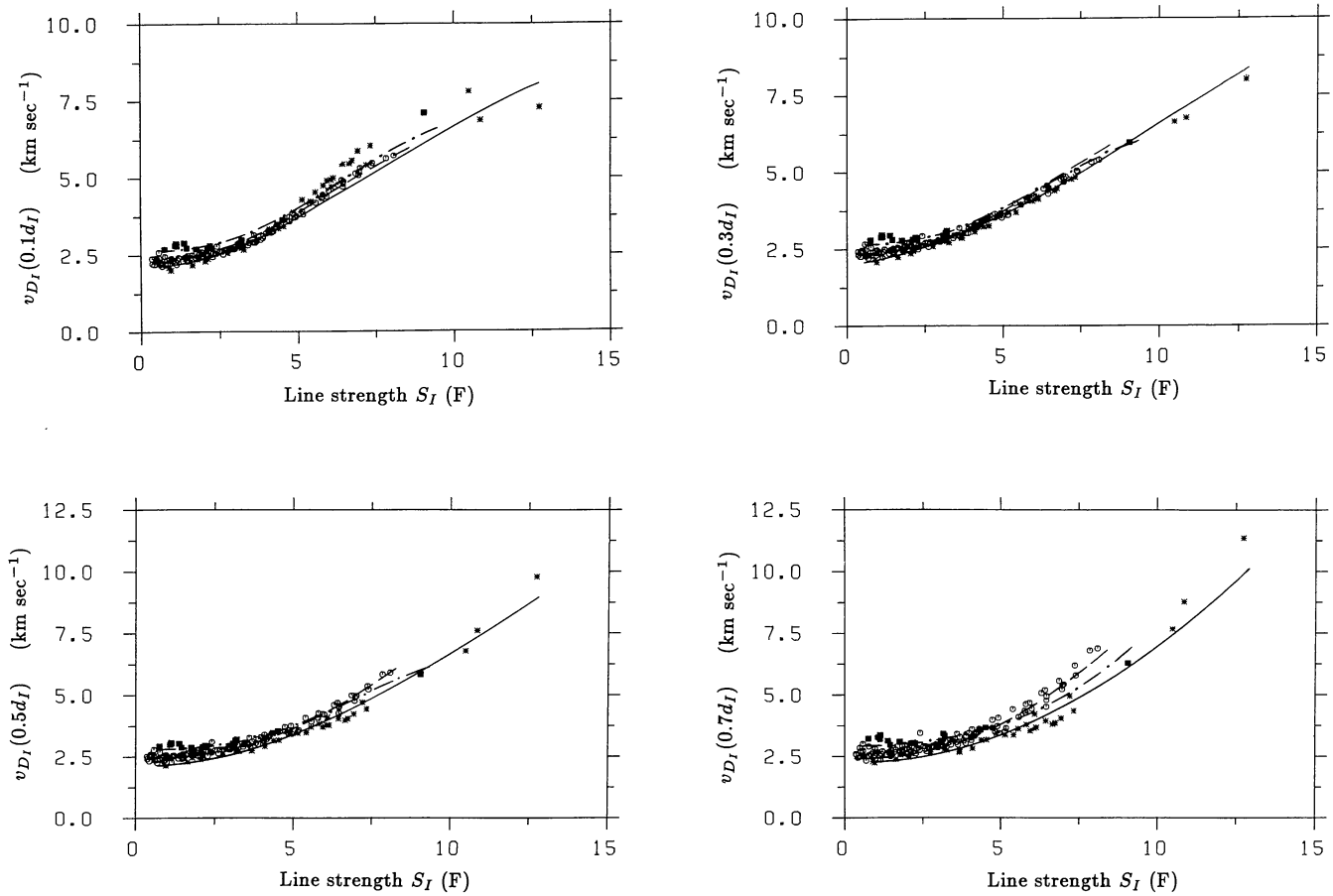

Fig. 4b. The four sub-figures show $v_{D_I}(0.1d_I)$ vs. S_I, $v_{D_I}(0.3d_I)$ vs. S_I, $v_{D_I}(0.5d_I)$ vs. S_I, and $v_{D_I}(0.7d_I)$ vs. S_I respectively. Here $v_{D_I}(0.1d_I)$ is the line width of Stokes I, in velocity units, at a level $0.1d_I$ above line bottom etc., expressed in velocity units in terms of the Doppler width of a Gaussian having the same width as Stokes I at the respective level. Quiet sun data and model calculations based on the HSRA. The data and the model results are denoted by the same symbols and curves as in Fig. 4a

© European Southern Observatory • Provided by the NASA Astrophysics Data System

1986A&A...168..311S

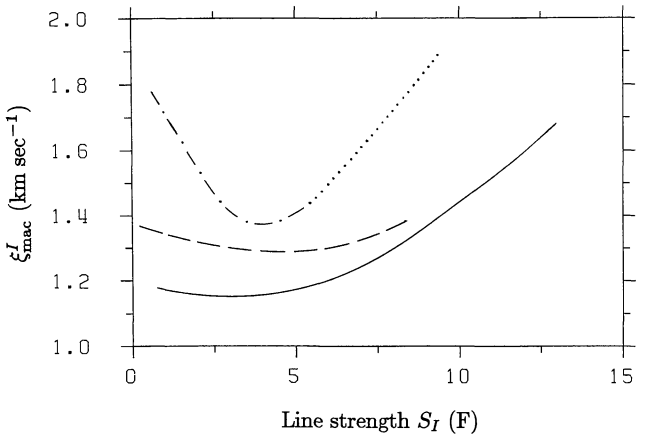

Fig. 5a. ξ^I_{mac}, the width of the 'Doppler core' of the macroturbulent velocity profile, as derived from Stokes I profiles observed in a quiet region, plotted vs. S_I. The ξ^I_{mac} values derived from Fe I lines with $\chi_e < 3$ eV are denoted by the solid curve, the ξ^I_{mac} values derived from Fe I, $\chi_e \geq 3$ eV lines by the dashed curve, and ξ^I_{mac} from Fe II by the dot-dashed curve. The Fe II curve is dotted between $S_I = 5$ and 9 F to indicate that it is interpolated in that region. $\delta_I = 2.5$

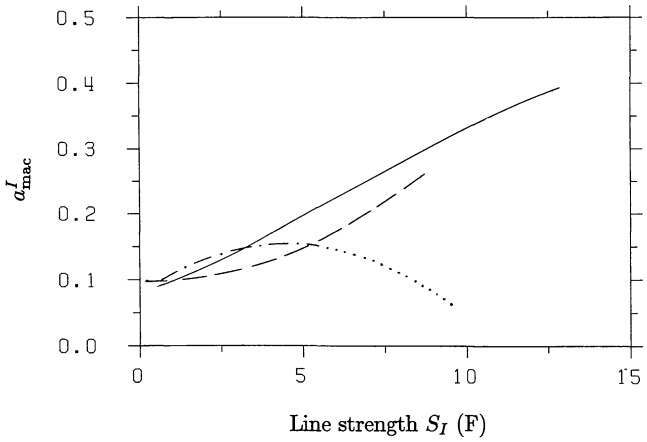

Fig. 5b. a^I_{mac}, the ratio of 'damping' to 'Doppler' width of the macroturbulent velocity profile plotted vs. S_I for the quiet sun. The symbols have the same meaning as in Fig. 5a

be noted that the rms velocity (for $a^I_{mac} = 0$) is $\xi^I_{mac}/\sqrt{2}$.[1] We also wish to point out that the ξ^I_{mac} and a^I_{mac} curves of Fe II are interpolated between $S_I = 5$ F and $S_I = 9$ F due to the absence of unblended Fe II lines in that range. This part of these curves is therefore dotted in Fig. 5 and in subsequent figures. The line parameters are sensitive to changes in ξ^I_{mac} at a level of about 0.1–0.2 km s^{-1}. The sensitivity to a^I_{mac} is of the order of 0.05–0.1. For smaller a^I_{mac} the fit to the five parameters is still quite good, and even $a^I_{mac} = 0$ reproduces the data reasonably well. The values of ξ^I_{mac} and a^I_{mac} needed to reproduce the observed profiles are compatible with those used by Smith et al. (1976) and Nordlund (1978) for a smaller number of lines. As a check and a further illustration the observed and calculated profiles of the Fe I 5127.7 Å, 5247.1 Å, 5383.4 Å lines and Fe II 5414.1 Å are shown in Fig. 6. The fit of these lines to the quiet sun Stokes I data is average in quality. Their observed line strengths, S_I, and the ξ^I_{mac} (km s^{-1}) and a^I_{mac} values used to broaden their model profiles are listed in Table 1. These are comparable to the values shown in Fig. 5 for lines of equal strength and similar excitation potential, which were obtained from fitting the line parameters alone.

[1] Due to an oversight this factor of $1/\sqrt{2}$ was forgotten by Solanki (1985). All the numbers in the section on velocities and in Fig. 2 of that paper should therefore be reduced by this factor in order to match the text.

4.3. *Fluxtube models with purely macroturbulent velocity broadening*

The analysis of Solanki and Stenflo (1984, Fig. 8) suggested that without mass motion induced broadening, the calculated profiles of lines formed in fluxtubes are much narrower than the observed profiles. Since our knowledge of the velocity structure inside fluxtubes is extremely rudimentary, we have decided, as a first step, to limit ourselves to determining the approximate rms velocity amplitudes involved, without modelling flows or oscillations in detail. Following the approach outlined in Sect. 4.2 for unpolarised radiation coming from the quiet photosphere, we shall assume that the non-thermal, non-magnetic line broadening inside fluxtubes is produced by macro- and microturbulent velocities. In this section we assume that macroturbulence alone is the broadening agent, and defer the study of the effects of adding a height independent microturbulent velocity until the next section. We must stress, that the use of a macroturbulent (and later also of a microturbulent) velocity does not signify that we assume the presence of true turbulent or convective motion inside the fluxtube. Rather, we use the turbulence velocity approach as a simple, convenient, and effective method of determining the line of sight amplitude of what may in reality be a highly complicated velocity field. Since the observations, which we use to empirically determine the velocities, were carried out near disk centre, and fluxtubes are expected to be nearly vertical due to buoyancy, the distortion due to geometrical effects should be small, and the line of sight velocity amplitude should be a good approximation of the total velocity amplitude. It must be borne in mind, however, that due to the averaging over time and over a number of fluxtubes, motions limited either to a small fraction of the fluxtubes in the resolution element, or to short timescales may have a negligible effect on the observed line width. However, line broadening can also capture motions which would not give rise to any Stokes V asymmetry, or to a net wavelength shift.

An idea of how the widths of the calculated lines compare with the observed ones can be obtained by plotting $v_{D_V} - v_{D_I}$ (line width difference at the 0.5d chord) vs. S_I for the observed and the calculated lines. An example is shown in Fig. 7a, where the I_V data are from a network region, the Stokes I data are taken from the quiet sun (to avoid filling factor effects), and the model curves are produced by subtracting the v_{D_I} values calculated in Sect. 4.2 from the line widths of the profiles of a network model with no internal velocity. The three curves correspond to the three sets of hypothetical iron lines, described in Sect. 4.1. The data have been reduced to the case of $g_{eff} = 0$ using the regression equation given by Solanki and Stenflo (1984). This regression mainly reduces the scatter in the data points without changing the form of the data curves significantly. It will be noticed that in general the model curves lie below the data, specially for the medium strong lines.

© European Southern Observatory • Provided by the NASA Astrophysics Data System

1986A&A...168..311S

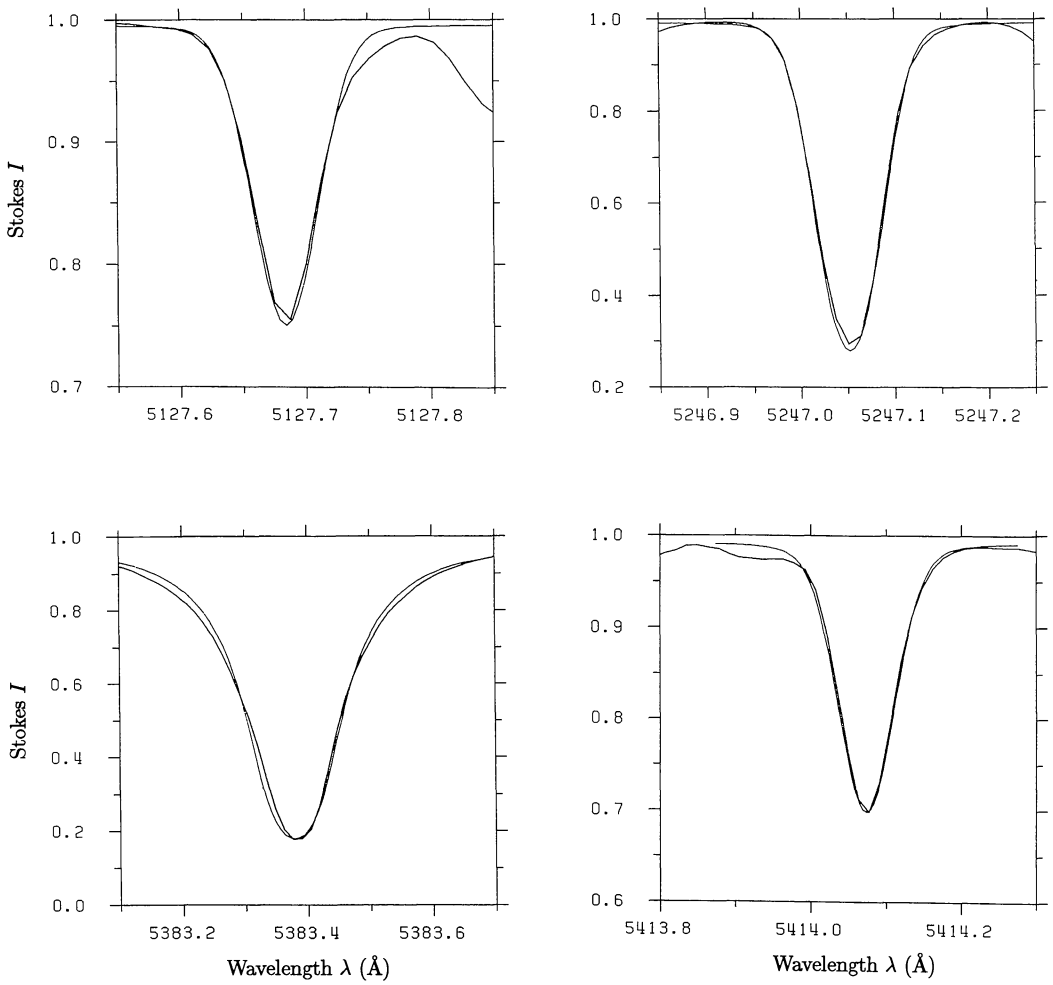

Fig. 6. Stokes I profiles of Fe I 5127.7 Å, 5247.1 Å, 5383.4 Å, and Fe II 5414.1 Å on the quiet sun. Observations: thick curves; synthetic profiles: thin curves

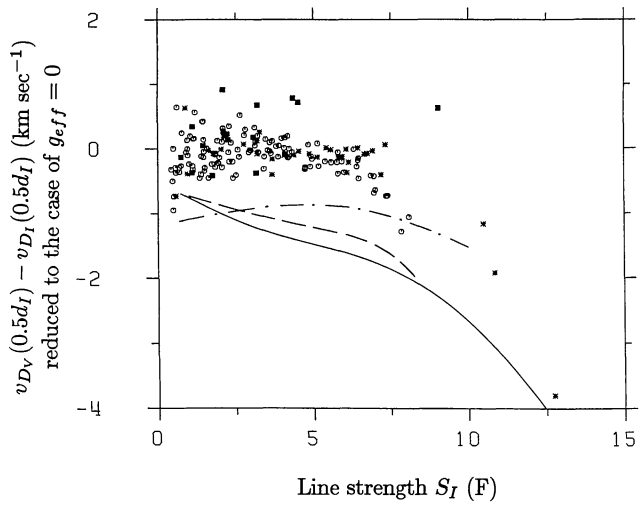

Fig. 7a. $v_{D_V} - v_{D_I}$, the difference between the half-widths of the I_V profile and of the Stokes I profile, reduced to the case of $g_{\text{eff}} = 0$, plotted vs. S_I. Symbols as in Fig. 4a. The data are from a network region and the calculations are based on a network fluxtube model. The calculated profiles are unbroadened by any velocity. $\delta_\Gamma = 2.5$

The relative positions between the model curves of different excitation lines also differ from the relative positions of the data points belonging to lines of different excitation potential. For example the observed high excitation Fe I lines show smaller $v_{D_V} - v_{D_I}$ values than the low excitation ones, while the model curves exhibit the opposite tendency. The observed I_V line widths and depths cannot be simultaneously reproduced for any fluxtube temperature structure if the synthetic profiles are not broadened by velocity. This statement was tested for $\delta_\Gamma = 1$ and $\delta_\Gamma = 2.5$, and was found to be true for both values within our grid of models.

Perhaps we should add that the difference in width between observed Fe I lines of equal S_I, but different excitation potentials, comes mainly from the fact that the Stokes I profiles of high excitation lines are broader than of the low excitation ones. The larger average width of the medium strong and strong Fe II lines compared to the Fe I lines, on the other hand, is due mainly to the difference between the V profiles of these lines, since the relative widths of the Stokes I profiles of Fe I and II lines would tend to produce the opposite effect in the $v_{D_V} - v_{D_I}$ vs. S_I diagram.

One potential source of error for the I_V line widths is the process by which the I_V continua have been renormalised (described in Sect. 2.3). To estimate the error which this process can intro-

© European Southern Observatory • Provided by the NASA Astrophysics Data System

1986A&A...168..311S

duce, we determined the half widths of the blue and red halves of unrenormalised lines and compared them to the half widths of the renormalised lines. We carried this out for a number of lines with large absolute and relative asymmetries. In all but one case the differences were considerably smaller than the scatter due to noise. This result leads us to believe that the Stokes V area asymmetry and our simple method of countering its effects do not have any appreciable effect on this analysis.

The fluxtube model line profiles are now broadened by convoluting them with a macroturbulence profile similar to the one chosen in Sect. 4.2. However, noise and the proximity of neighbouring lines usually make damping wings in Stokes V very hard to measure accurately (one should also keep in mind that $V \sim \partial I/\partial\lambda$, which is small in the damping wings of the line), so that, to the degree of accuracy we are interested in, $a^V_{\rm mac}$ can usually be neglected. We therefore set $a^V_{\rm mac} = 0$, i.e. we choose a purely Gaussian macroturbulent velocity profile inside the fluxtube. By choosing the values of $\xi^V_{\rm mac}$ (i.e. $\xi_{\rm mac}$ as determined from the I_V profile) properly, the calculated line widths can be made to match the observed ones almost perfectly, as is demonstrated in Fig. 7b.

To see how strongly the empirical $\xi^V_{\rm mac}$ values depend on the assumed temperature structure, a number of models with different $T(\tau)$ functions were calculated with temperatures ranging from 200 K higher than the photospheric value at equal τ, to approximately 1000 K higher in the part of the atmosphere where the lines of interest are formed. Some models (with too low temperatures) resulted in a part of the lines being too broad to be compatible with the observations even without velocity broadening, but for the rest of the models, despite differences in detail, the velocities obtained were surprisingly similar. Within the above temperature range, which is wide enough to encompass the temperature structure of almost all empirical fluxtube models, the $\xi^V_{\rm mac}$ values remain constant to within, on the average, $\pm 0.5\,{\rm km\,s^{-1}}$. The sensitivity of the derived $\xi^V_{\rm mac}$ value to the temperature is a function of the line strength, with the $\xi^V_{\rm mac}$ values derived from the weakest lines being constant to within 0.1–$0.2\,{\rm km\,s^{-1}}$, whereas for the strongest Fe I lines $\xi^V_{\rm mac}$ can vary by up to $\pm 1.5\,{\rm km\,s^{-1}}$ within this temperature range. This dependence on line strength may be explained by the increasing sensitivity of line width on temperature with the increasing importance of saturation effects.

The maximum values of $\xi^V_{\rm mac}$ for plage data and $\delta_\Gamma = 1$ vary between 3.2 and $4.4\,{\rm km\,s^{-1}}$ for Fe I lines with $\chi_e = 1.5\,{\rm eV}$, between 2.5 and $3.5\,{\rm km\,s^{-1}}$ for Fe I lines with $\chi_e = 4\,{\rm eV}$, and between 3.6 and $4.9\,{\rm km\,s^{-1}}$ for the Fe II lines. The general trend for all the models being for the velocity amplitude to increase with increasing line strength for the weak and medium strong lines ($S_I \lesssim 8$–10 F), but to even out and eventually to decrease again for the strongest lines. The $\xi^V_{\rm mac}$ values for the network show a similar trend, but are lower than the velocities found in plages by, on the average, 0.3–$0.5\,{\rm km\,s^{-1}}$, if we assume the *same temperature structure* for the fluxtubes in both regions. The difference in velocity is only an artifact of this assumption of equal temperature and disappears when we model fluxtube temperatures more realistically (see below).

Of course, our aim is to reproduce not just the widths of the observed I_V profiles, but their depths as well. After having ascertained how the macroturbulence affects the line profiles for the initial grid of models, we started searching for a temperature model giving a reasonable representation of the complete line profiles of all the observed lines. As a starting point, the models found by Solanki (1984) to give a good fit to the $\ln(d_V/d_I)$, vs. S_I plot of the data were chosen. However, for a number of reasons, these models had to be modified. Firstly, they had been derived from fits to the line depths only, without taking the line widths into account, so that when the calculated profiles are convoluted with a macroturbulence to reproduce the observed line widths, the good fit to the line depths is lost. Secondly, the photospheric lines had been fitted by using a depth dependent *micro*turbulence alone in the previous work. The microturbulence inside the fluxtube had been assumed to be simply some fixed fraction (typically 0.5–0.7) of the photospheric microturbulence. Since we do not assume any microturbulence at all inside the fluxtube in this section, this will also change the inferred temperature structure slightly. Finally, the inclusion of atmospheric layers above the temperature minimum in the model changes the calculated profiles of the strongest lines somewhat.

However, some basic characteristics of the earlier models remain. For example the difference between the temperature of plage and network fluxtubes found earlier is confirmed by the new models, with network fluxtubes being hotter than plage fluxtubes. The depression in temperature at some τ value, where it falls almost to the quiet sun value at that τ, found as a unifying characteristic in the earlier models (cf. Solanki, 1984) is still visible, although it is decidedly weakened. The ambiguity in temperature structure as determined by Fe I and II lines alone, which was pointed out by Solanki (1984), still appears to be present, although we have not carried out such extensive test calculations as in the previous work.

The temperature structures of network and plage models giving rise to best fit line profiles are shown in Fig. 8 as a function of τ_{5000}, the continuum optical depth at 5000 Å. The HSRASP temperature structure is also shown for comparison. We wish to stress that these temperature models are of a preliminary nature, it not being the aim of this paper to investigate the $T(\tau)$ structure of fluxtubes. Additional data containing better information on levels below $\log\tau = -1$ and above $\log\tau = -3$, as well as improved modelling techniques (1.5D radiative transfer etc.) are required.

How such a model (network), combined with macroturbulence broadening, reproduces $v_{D_V} - v_{D_I}$ vs. S_I has already been

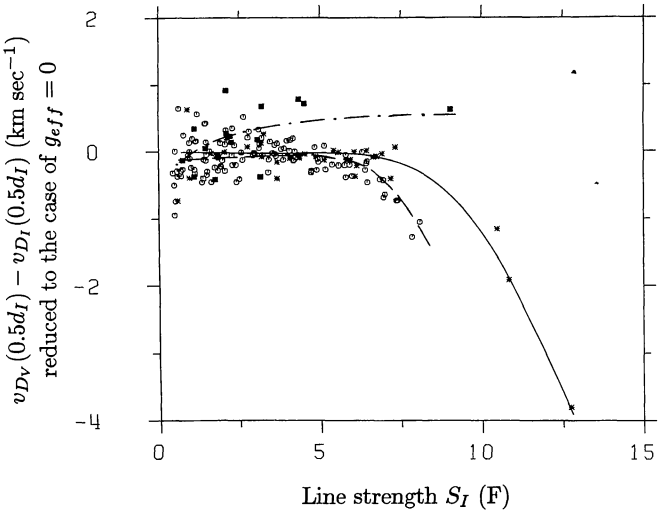

Fig. 7b. The same as Fig. 7a, except that the calculated profiles have been broadened by a macroturbulence to make them match the data

© European Southern Observatory • Provided by the NASA Astrophysics Data System

1986A&A...168..311S

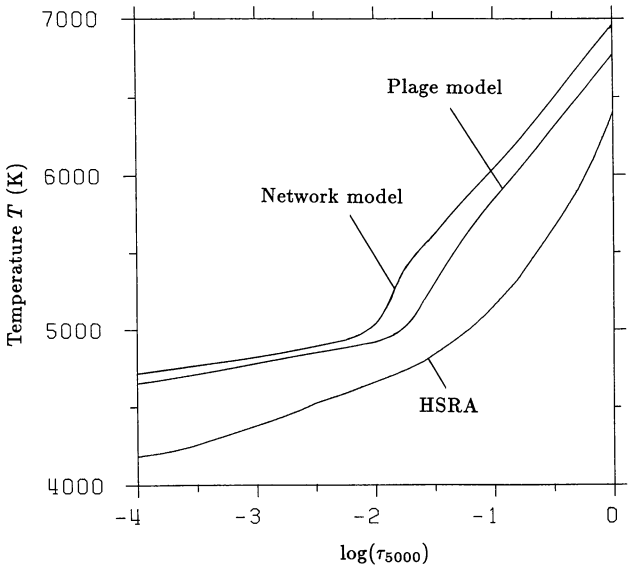

Fig. 8. The temperature T in K vs. the logarithm of the optical depth $\log(\tau_{5000})$ for the HSRASP (see text), and for a model each of fluxtubes in the network and in active region plages. These models have been used to calculate the best fit profiles presented in Figs. 7b, 9, etc.

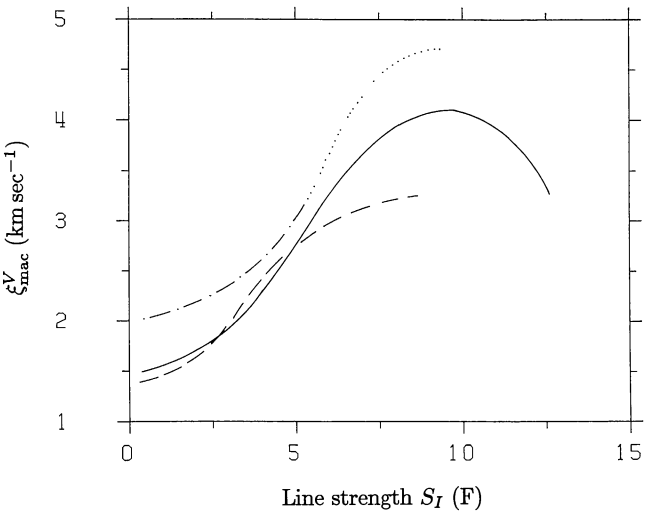

Fig. 10. $\xi^V_{\rm mac}$, the macroturbulence velocity derived from the I_V profile, vs. S_I. Plotted are the results for both network and plage data, if $\xi_{\rm mic} = 0$, and $\delta_\Gamma = 1$. $a^V_{\rm mac} = 0$ is assumed for all fluxtube models. Symbols as in Fig. 5a

illustrated in Fig. 7b. Figure 9 shows how well the same model reproduces the $\ln(d_V/d_I)$ vs. S_I data from the same network region. A fit of similar accuracy was also obtained for the plage data. In Fig. 10 $\xi^V_{\rm mac}$ is plotted vs. S_I, for both the best fit plage and network models. Since the plage velocities are almost the same as the velocities in the network fluxtubes, only one curve has been drawn for each group of lines. The scatter in the data limits the accuracy of our $\xi^V_{\rm mac}$ curves to approximately ± 0.3–$0.5\,{\rm km\,s^{-1}}$. The relative values of $\xi^V_{\rm mac}$ for the Fe I low χ_e, high χ_e, and Fe II lines are consistent with Fig. 7a. The large difference in line widths between the Fe II data and profiles calculated from velocity free models gives rise to a large $\xi^V_{\rm mac}$. For high excitation Fe I lines, on the other hand, the data and model curves in Fig. 7a lie relatively close together, so that $\xi^V_{\rm mac}$ for those lines is small.

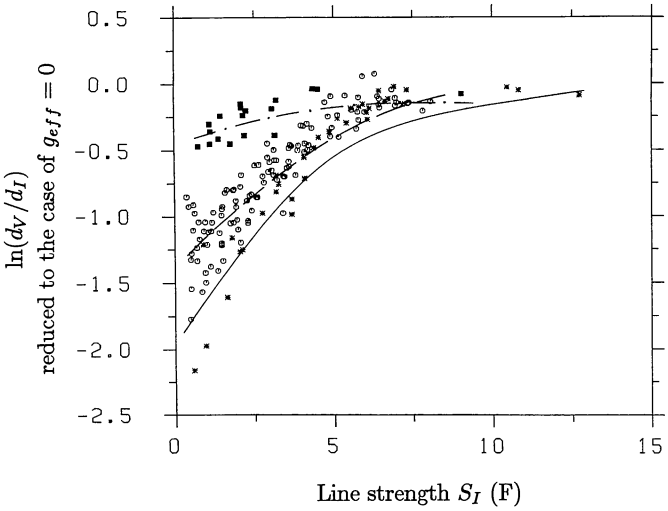

Fig. 9. $\ln(d_V/d_I)$, the natural logarithm of the ratio between the line depths of I_V and Stokes I, plotted against S_I. Symbols as in Fig. 4a. The calculated line profiles have been convoluted with a macroturbulent velocity. The data were obtained in a network region, the model is the same as in Fig. 7b. $\delta_\Gamma = 2.5$

A comparison of Fig. 10 with Fig. 5a shows strikingly, that the dependence of the velocity on line strength in the fluxtube is quite different from that in the photosphere. The initial value of $\xi^V_{\rm mac}$ is roughly similar to $\xi^I_{\rm mac}$ (Fig. 5a), but becomes considerably larger than $\xi^I_{\rm mac}$ for larger S_I. However, one should keep in mind that for the quiet sun we used a Voigt function ($a_{\rm mac} \neq 0$) for the velocity distribution, so that the $\xi^I_{\rm mac}$ values cannot be directly compared to $\xi^I_{\rm mac}$. We shall return to this point in Sect. 5.

Figure 11 illustrates the effect on $\xi^V_{\rm mac}$ of increasing the damping constant by a factor of 2.5. As expected, the weak lines remain virtually unaffected by this change while the $\xi^V_{\rm mac}$ values for the strong lines are considerably reduced. Small differences between $\xi^V_{\rm mac}$ of the weak lines result from the fact that the temperature had to be changed slightly between models with different δ_Γ to retain the quality of the fit to the $\ln(d_V/d_I)$ plot. The velocities obtained now from the strong lines in the network are larger than those found in the plage regions. This is consistent with the case of $\delta_\Gamma = 1$ (Fig. 10), since the increase in damping constant will more strongly broaden the lines in a plage, these being less weakened than their network counterparts due to the lower temperature in the plage. Models with $\delta_\Gamma = 2.5$ reproduce the data somewhat better than models with $\delta_\Gamma = 1$ and Figs. 7b and 9 actually show the results of such models. From Figs. 10 and 11 we see that the photospheric sound speed (9–$10\,{\rm km\,s^{-1}}$) is larger than the maximum rms velocity in fluxtubes (3–$3.5\,{\rm km\,s^{-1}}$) by a factor of about 3. This result is consistent with the initial assumption that the structure of the fluxtubes is not critically affected by any motions occuring inside them.

Finally Fig. 12 shows the I_V profiles, observed in a plage, of the three Fe I lines at 5127.7 Å, 5247.1 Å, and 5383.4 Å and the Fe II 5414.1 Å line, together with their calculated Stokes I profiles from the best fit plage model. Fe II 5414.1 Å and Fe I 5383.4 Å are the two worst fit profiles in our sample, whereas the other two figure among the better reproduced lines. The correspon-

© European Southern Observatory • Provided by the NASA Astrophysics Data System

1986A&A...168..311S

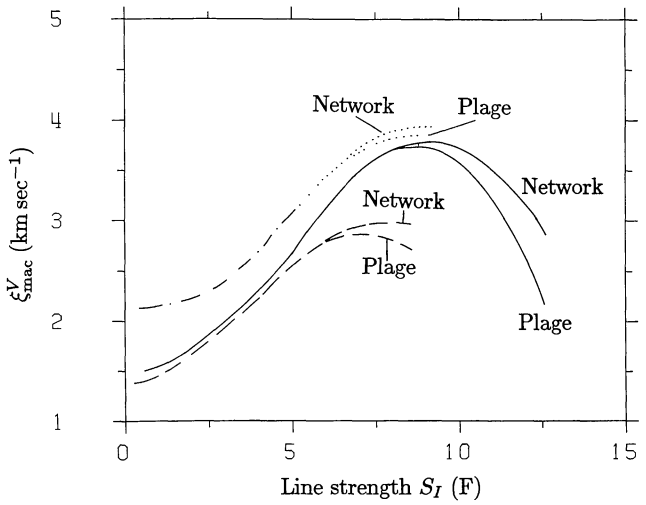

Fig. 11. ξ^V_{mac} vs. S_I with $\xi_{mic} = 0$, and $\delta_I = 2.5$. The different groups of lines are denoted as in Fig. 5a. The lower curve for each group of spectral lines represents a plage region, the upper curve a network region

dence for all ten lines is quite reasonable, considering the fact that some distortion of the I_V profile due to noise and Stokes V asymmetry is bound to occur. The ξ^V_{mac} values used to broaden the synthetic profiles are listed in the final column of Table 1 ($a^V_{mac} = 0.0$ and $\delta_I = 2.5$). These values lie quite close to those derived from hypothetical lines of the same strength, which are shown in Fig. 11. The Fe I 5250.2 Å lines is also reproduced with an accuracy similar to Fe I 5247.1 Å, a somewhat surprising result, since its large Landé factor of 3 would lead one to expect that the first order approximation on which the calculation of the I_V profile is based may be insufficient for this line.

Could these non-thermal line broadenings have a non-solar source? The line broadening induced by changes in relative observer-source velocity is negligible ($\approx 50\,m\,s^{-1}$, Sect. 2.2). This is also true of smearing due to finite spectral resolution. Anyway, both these processes affect I_V and Stokes I equally and therefore have no influence on our analysis. We have seen that the renormalisation of the continuum of I_V necessitated by the area asymmetry of Stokes V, does not have a large effect on its half width. Another possibility is that the first order approximation, on which the I_V profile is based, it not accurate enough for the detailed analysis of the line widths. If this were the case, then we would expect the line widths of the I_V profiles to be strongly dependent on their Landé factors, since the quality of the approximation is better, the smaller the ratio of Zeeman splitting to Doppler width of the line. The dependence of I_V line width on Landé factor has been studied by Solanki and Stenflo (1984) who find that the widths of the I_V profiles increase with Landé factor exactly as expected in the presence of a kilogauss magnetic field. This, and the fact that the same ξ^V_{mac} value is required to

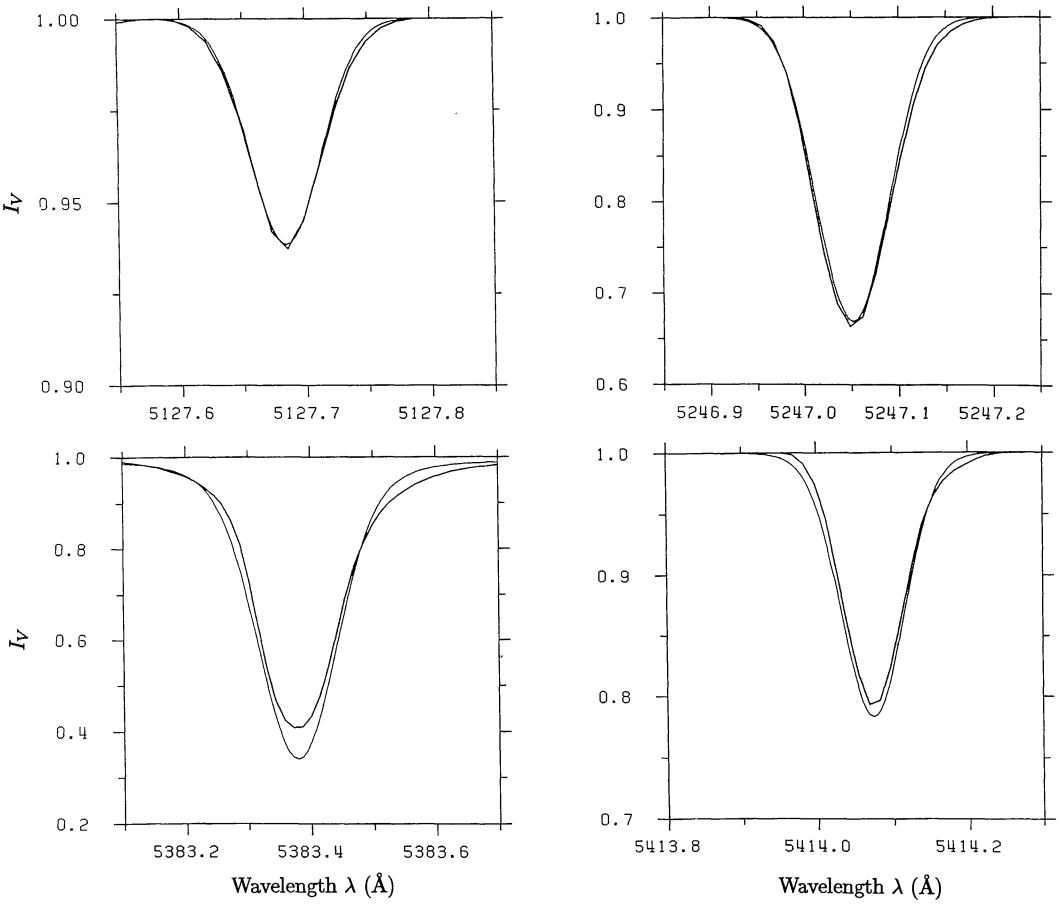

Fig. 12. The observed (I_V) and calculated profiles of the Fe I 5127.7 Å, 5247.1 Å, 5383.4 Å, and Fe II 5414.1 Å lines for a plage. I_V data: thick curves. Synthetic profiles: thin curves

© European Southern Observatory • Provided by the NASA Astrophysics Data System

1986A&A...168..311S

reproduce the observed profiles of Fe I 5250.2 Å and Fe I 5247.1 Å (cf. Table 1) leads us to conclude that the anomalously large I_V line widths have a solar origin.

4.4. *Effects of adding microturbulence*

The observed Stokes V asymmetry suggests that at least a part of the motions in magnetic fluxtubes may be non-uniform over the typical range of formation of a spectral line. This non-uniform component may be better approximated by microturbulence than by macroturbulence. Therefore, we shall describe the results of some fluxtube model calculations which use a mixture of microturbulence and macroturbulence. In principle it is possible to fit a line profile with either a mixture of macroturbulence and depth independent microturbulence, or with a depth dependent microturbulence alone (Holweger et al., 1978). However, no new physical insight is gained by using the second approach, and it is considerably more time consuming to carry out, since all the line profiles have to be recalculated for each trial depth dependence of the microturbulence, instead of simply being convoluted with different velocity profiles after being calculated once and for all for each chosen temperature structure, as is the case for the macroturbulence. We have therefore restricted ourselves to the case of a depth *in*dependent microturbulence.

Figure 13 shows the effect of introducing a depth independent microturbulent velocity, $\xi_{\rm mic}$, on the macroturbulence $\xi^V_{\rm mac}$. Figure 13a shows $\xi^V_{\rm mac}$ as derived by fitting the Fe I, $\chi_e < 3$ eV data with Fe I, $\chi_e = 1$ eV lines calculated for models with $\xi_{\rm mic} = 0$, 0.5, 1 and 1.5 km s^{-1} respectively. $\delta_T = 2.5$ for all four models, and the temperature structure is also the same for all the models. The data are from a network region. As expected, $\xi^V_{\rm mac}$ decreases as $\xi_{\rm mic}$ is increased. For weak lines the decrease is such that $(\xi^V_{\rm mac})^2 + (\xi_{\rm mic})^2$ remains approximately constant, so that the total turbulent velocity remains unchanged. For the strong lines this is no longer the case. There $\xi^V_{\rm mac}$ decreases much faster, and the total turbulent velocity also decreases. This is due to the fact that increasing $\xi_{\rm mic}$ increases the strength of the lines. This increase, and the associated increase in line width is strongly dependent on the equivalent width of the line, being largest for lines with $W_\lambda \approx 80$ mÅ at disk centre (Holweger et al., 1978). Although the strongest Fe I lines in our sample have large equivalent widths on the quiet sun ($W_\lambda > 100$ at disk centre), and according to Holweger et al. (1978) should not be strongly affected by the microturbulence, they are weakened in fluxtubes and thus come into the range of lines having a large sensitivity to $\xi_{\rm mic}$. Figure 13a also shows that assuming $\xi_{\rm mic}$ to be the same at all heights, 1.5 km s^{-1} is the largest value it can have at disk centre, since for this value of $\xi_{\rm mic}$, $\xi^V_{\rm mac}$ falls to zero for both the weakest and the strongest Fe I lines. $\xi_{\rm mic}$ values larger than that would cause these lines to be broader than the observed values, even for $\xi^V_{\rm mac} = 0$. Although we have tested this result for only one temperature structure, the relative insensitivity of the widths of weak lines to temperature means that it should retain its validity for a reasonable range of temperatures.

Figure 13b and 13c are similar to Fig. 13a, except that they show the results derived from the Fe I lines with $\chi_e = 4$ eV and the Fe II lines respectively. The high excitation Fe I lines also give a maximum $\xi_{\rm mic}$ value of 1.5 km s^{-1}, but the Fe II lines would allow for higher microturbulence velocities.

We can improve on the limit for $\xi_{\rm mic}$ simply by observing how well the model curves fit the $v_{D_V} - v_{D_I}$ vs. S_I and $\ln(d_V/d_I)$ vs. S_I data simultaneously. We find that the data as represented by these plots are best reproduced by the models with $\xi_{\rm mic} =$ 0.5 km s^{-1} and 1.0 km s^{-1}, which give fits slightly better than those shown in Fig. 7b and Fig. 9.

For plage data the effect of $\xi_{\rm mic}$ is qualitatively the same. The resulting maximum value for $\xi_{\rm mic}$ is again 1.5 km s^{-1}, and $\xi_{\rm mic}$ between 0.5 and 1.0 km s^{-1} once more gives the best fit to the data. It therefore appears that whereas the macroturbulence velocity inside the fluxtubes can reach values considerably higher than in the quiet photosphere, the microturbulence velocity is of the same order.

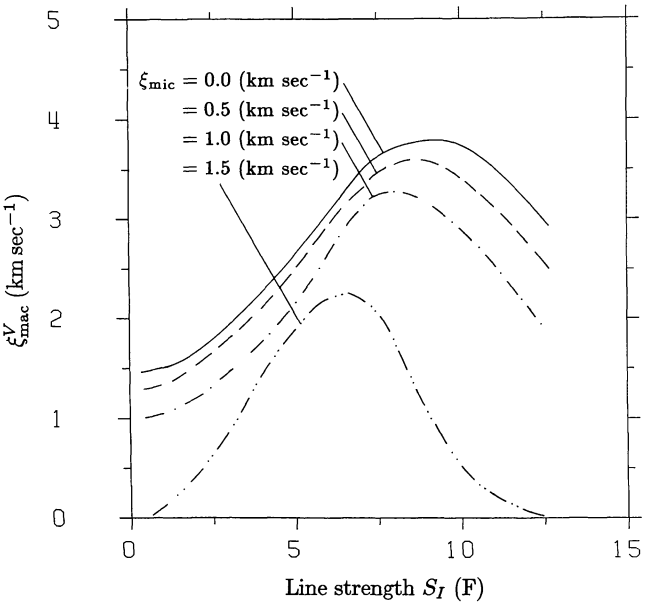

Fig. 13a. $\xi^V_{\rm mac}$ vs. S_I for network data and models. Fe I lines with $\chi_e <$ 3 eV. The different curves are, from top to bottom, for models with microturbulence, $\xi_{\rm mic} = 0$, 0.5, 1.0, and 1.5 km s^{-1}. $\delta_T = 2.5$

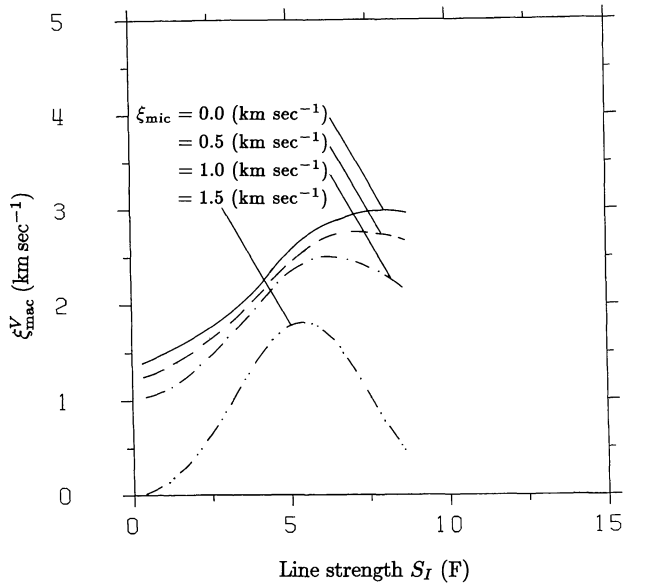

Fig. 13b. The same as Fig. 13a for Fe I lines with $\chi_e \geq 3$ eV

© European Southern Observatory • Provided by the NASA Astrophysics Data System

1986A&A...168..311S

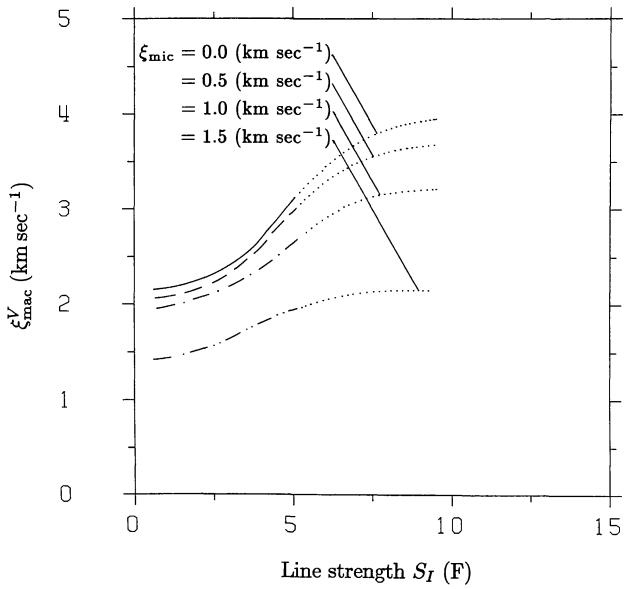

Fig. 13c. The same as Fig. 13a for Fe II lines

4.5. The relation between Stokes V asymmetry and line width

The possible existence of a relation between the Stokes V asymmetry and the width of the I_V profile was first suggested by Solanki and Stenflo (1984). Solanki (1985) presented additional evidence in favour of this hypothesis by pointing out the similarity between the ξ^V_{mac} vs. S_I and the $a_b - a_r$ vs. S_I diagrams, a_b and a_r being the absolute values of the Stokes V blue and red amplitudes. We would like to put this analysis on a more quantitative footing. Figure 14 shows ξ^V_{mac} (derived assuming $\xi_{mic} = 0$) plotted vs. $a_b - a_r$, both quantities having S_I as a parameter. The S_I values 0, 2.5, 5, 7.5, 10, and 12.5 F are marked by notches in the curves. For the Fe II lines the point at $S_I = 9.3$ F is marked instead of $S_I = 7.5$ F. The Fe II curve between $S_I = 5$ F and $S_I = 9.3$ F is dotted to indicate that it is interpolated between those values. The asymmetry data and ξ^V_{mac} values are for an enhanced network region. The model for which ξ^V_{mac} is derived, is the best fit network model with $\xi_{mic} = 0$ and $\delta_T = 2.5$. The peculiar hook-like shape of the curves is due to the decrease in asymmetry and ξ^V_{mac} above $S_I \approx 7$–8 F, and is without deeper significance, being only an artifact of plotting the data with S_I as a parameter. The straight line is a least-squares fit to the three curves. A straight line fit to the data is also suggested by comparing Fig. 2 of Solanki (1985) with his Fig. 3, or equivalently by comparing Fig. 3 of Solanki and Stenflo (1985) with Fig. 11 of the present paper.

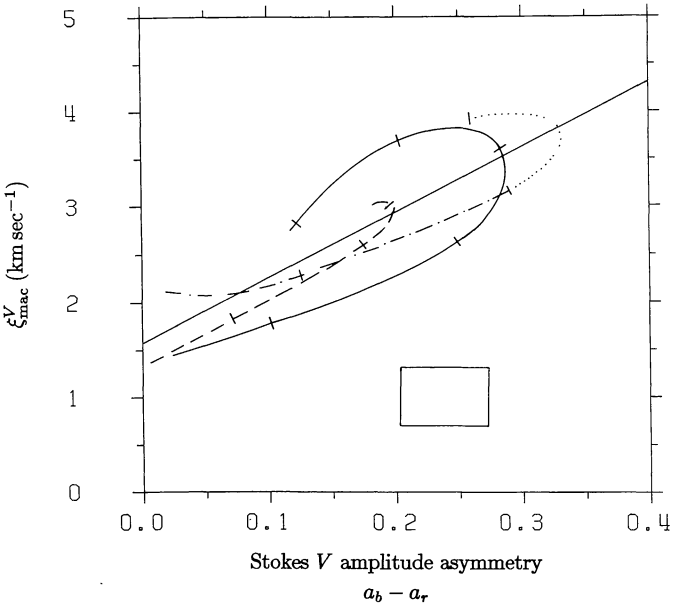

Fig. 14. ξ^V_{mac} vs. $a_b - a_r$, where $a_b - a_r$ is the absolute amplitude asymmetry of Stokes V. The curves are plotted with S_I as a parameter. Its value is marked by notches every 2.5 F. The different groups of spectral lines are represented in the same manner as in Fig. 5a. An error box is plotted at lower right

The correlation coefficient for these two quantities is 0.85 (on a scale ranging from -1 to $+1$, with ± 1 meaning perfect correlation, and 0 a total absence of correlation), which is high enough to suggest the existence of a simple linear relation between the fluxtube velocity amplitudes, as determined from the line broadening, and the asymmetry of Stokes V, specially if we take the rather large errors, indicated by the error box in the lower right of the figure, into account. Its size is primarily dictated by the considerable scatter in the asymmetry values of the different lines.

It is interesting to note that the asymmetry tends to disappear for very weak lines, while the velocity broadening does not. The least squares fit gives $\xi^V_{mac} = 1.6\,\mathrm{km\,s^{-1}}$ for $a_b - a_r = 0$.

5. Discussion and conclusions

In this paper we have attempted to empirically determine velocities in the photospheric layers of small solar magnetic fluxtubes. To achieve this aim we have mainly made use of the velocity information contained in two parameters derived from the Stokes V profile; its zero-crossing wavelength, λ_V, and the half-width, v_{D_V}, of the integrated V profile, I_V. λ_V is mainly sensitive to 'global' flows; global in the sense that the majority of the fluxtubes in the observed region show a line of sight flow in the same direction over most of the integration time of the observations. v_{D_V}, on the other hand, is mainly sensitive to vertical velocity gradients and (statistical) fluctuations of the velocity in space or time, as may result for example from oscillations or waves in a fluxtube, or from the presence of different flow velocities in a number of fluxtubes.

We find no zero-crossing shifts larger than approximately $\pm 250\,\mathrm{m\,s^{-1}}$ in any of the observed regions (including both active region plages and network elements near disk centre) for a large sample of unblended Fe I and II lines, as well as the Mg Ib lines at 5172 Å and 5183 Å. This allows us to set an upper limit of this amount on steady up- and downflow velocities in magnetic fluxtubes. The limit in accuracy of approximately $250\,\mathrm{m\,s^{-1}}$ is imposed by uncertainties in the determination of the absolute wavelength of the V profiles, and partly also by the scatter in the data points. This limit is totally *independent* of the wavelength of the simultaneously measured Stokes I profile, since it results from the comparison of absolute Stokes V wavelengths with the laboratory wavelengths of the respective lines.

A small dependence on line strength, Landé factor, and excitation potential of the Stokes V zero-crossing shift is observed, suggesting that the true line shifts are not exactly zero for all the

© European Southern Observatory • Provided by the NASA Astrophysics Data System

1986A&A...168..311S

lines. However, they remain much smaller than the large redshifts reported in a number of previous studies (e.g. Giovanelli and Slaughter, 1978; Wiehr, 1985). Solanki and Stenflo (1986) explain this discrepancy between the results of this and some previous studies by taking the difference in spectral resolution between the various observations into account. They show that the smearing of the Stokes V profiles due to insufficient spectral resolution, when combined with their asymmetry, leads to fictitious redshifts. By using the approximate instrumental parameters which have been used to observe the large downflows reported in the literature, they are able to reproduce the observed downflows to a reasonable degree of accuracy. The different measurements in the literature have been discussed in depth in that paper and we refer to it for further details. The observational case for large downflows inside fluxtubes is therefore considerably weakened and from a theoretical point of view, no need for *large* flows inside fluxtubes appears to exist as well, as has been argued for example by Durrant (1977). Schüssler (1986) estimates the velocity of the downflow induced by mass inflow into the tube due to diffusion across the field lines. He finds that downflows of the order of $10\,\mathrm{m\,s^{-1}}$ are expected for fluxtubes with radii of around 100 km, which is perfectly compatible with our results. The siphon flow mechanism has been discussed as a possible source for downflows by Hasan and Schüssler (1985), who conclude that it is unlikely to give rise to appreciable net downflows in small fluxtubes. Further, Ribes et al. (1985) find that a downflow velocity increasing with depth, as suggested by Giovanelli and Slaughter (1978), results in line profiles of a shape quite incompatible with the observations.

We therefore conclude that the mean steady flow velocities in the photospheric layers of small magnetic fluxtubes are smaller than approximately $250\,\mathrm{m\,s^{-1}}$, in both active region plages and the network. This limit is compatible with the substantial velocities observed in the transition region above active regions, even in the presence of magnetic canopies. Of course our analysis does not rule out the possibility of strong flows occuring inside fluxtubes under certain circumstances, for example in connection with their convective collapse, our observations being restricted to mature active regions and the enhanced network.

The comparison between λ_V and Stokes I core wavelengths, λ_I, tends to confirm the conclusion that if flows are present at all inside fluxtubes, then they are small. It suggests that their velocity is less than approximately $200\,\mathrm{m\,s^{-1}}$. It also provides support for the observation of Cavallini et al. (1984) that the granular blueshift of Stokes I is reduced by 100–$200\,\mathrm{m\,s^{-1}}$ in active regions.

How are the small observed Stokes V shifts to be interpreted, if lines with positive as well as negative wavelength shifts may occur in the same region? The dependence of line shift on line strength, wavelength and excitation potential is well known for the Stokes I profile, and has been convincingly explained by the correlated velocity and temperature structure of the convective cells associated with granules (Dravins et al., 1981). We suggest that the wavelength shifts observed for the Stokes V profiles may be the result of a similar mechanism. Of course, due to the strong magnetic field in fluxtubes all motions must be along the field lines, so that instead of convective motions we have oscillations. These oscillations (or waves) will require respectable amplitudes and a correlation between flow velocity and temperature, even if, like the five minute oscillations, they are coherent in all the fluxtubes of an observed region. This requirement is set by the long integration times of our observations, which ensure that the five minute oscillations are practically averaged out. The present analysis hints at the danger of interpreting small shifts ($\lesssim 300\,\mathrm{m\,s^{-1}}$) of the Stokes V profile of a single line as being evidence for a stationary up- or downflow inside a fluxtube, since lines with positive and negative shifts may be present in the same observed region, and also since even data with such long integration times and gathered over such a large region as ours still show a significant scatter.

That fluxtubes are not totally devoid of mass motions, also follows from the analysis in the second part of this paper, where line profiles calculated in a fluxtube model atmosphere are compared with the data. It is found that a broadening due to velocity is required in order to reproduce the observations. We have approximated the velocity field influencing the polarized light by assuming it to be composed of Gaussian macro- and microturbulent velocity profiles. We stress once more that we do not thereby imply the presence of true turbulence or of convective motion inside the fluxtubes. Macro- and microturbulence have only been chosen due to their effectiveness and simplicity of use. Total rms turbulent velocities of between approximately 1 and $3.5\,\mathrm{km\,s^{-1}}$ are derived from the I_V spectra, depending on the strength and the excitation potential of the line. Interestingly, plage and network model I_V profiles require essentially the same amount of velocity broadening to fit the data (if the appropriate temperature models are used), suggesting that the velocity structures of fluxtubes in the two types of regions are very similar.

The dependence of ξ_{mac} on the line strength is quite different for the magnetic and the non-magnetic data. This is best illustrated in Fig. 15, where the difference between ξ^V_{mac} for a network fluxtube and ξ^I_{mac} for the quiet sun is plotted vs. S_I. Both ξ^I_{mac} and ξ^V_{mac} have been determined using models with $\xi_{\mathrm{mic}} = 0.8\,\mathrm{km\,s^{-1}}$ and $a_{\mathrm{mac}} = 0$. We are therefore comparing like with like (at the cost of a slightly worse fit to the quiet sun data than with $a^I_{\mathrm{mac}} \neq 0$). As expected, ξ^V_{mac} is larger than ξ^I_{mac} for most of the lines. The near similarity in ξ^I_{mac} and ξ^V_{mac} for the weak lines is probably only due to their relative insensitivity to velocity broadening. One problem with such a comparison, specially for the Fe I lines, is that since they are considerably weakened inside the fluxtube, their sensitivity to velocity broadening is also changed. This could falsify the picture given by Fig. 15 somewhat. However, since for most lines the sensitivity decreases as they are weakened, this would tend to *under*estimate $\xi^V_{\mathrm{mac}} - \xi^I_{\mathrm{mac}}$, so that the effect may in reality be even larger.

We have also studied the effects of different temperature structures on the empirically determined velocity, and find that within reasonable limits of the temperature variation (i.e. over a range of about 800 K at a fixed τ value), the macroturbulence velocity remains on the average constant to within $\pm 0.5\,\mathrm{km\,s^{-1}}$.

Calculations based on the assumption that part of the velocity in the fluxtube is better represented by a microturbulence show the expected decrease in ξ^V_{mac} with increasing ξ_{mic}. The data set an upper limit of $1.5\,\mathrm{km\,s^{-1}}$ on ξ_{mic} in fluxtubes, assuming that it is height independent. Best values for ξ_{mic} appear to lie between 0.5 and $1.0\,\mathrm{km\,s^{-1}}$.

In Sect. 4.3 it was shown that the large I_V line widths are not an artifact of the method of data analysis, or of the long integration times, or the spectral resolution. They are therefore of solar origin. An obvious solar source are the five minute oscillations. These have been measured in Stokes V by Giovanelli et al. (1978) who find amplitudes of about $0.25\,\mathrm{km\,s^{-1}}$ for lines

© European Southern Observatory • Provided by the NASA Astrophysics Data System

1986A&A...168..311S

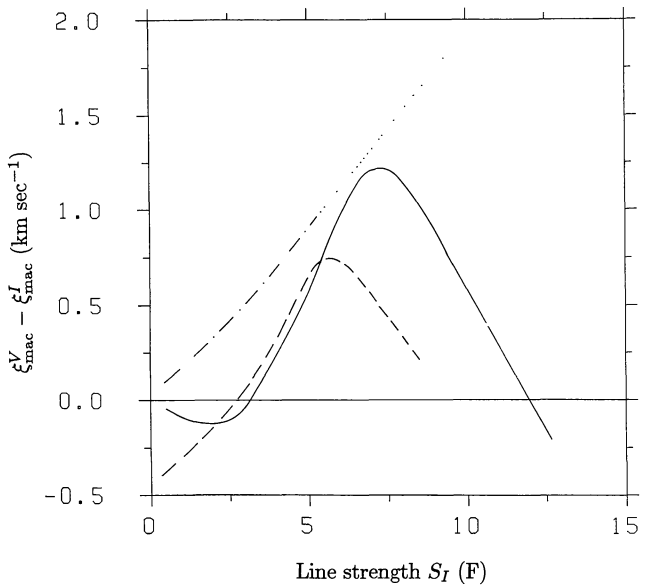

Fig. 15. $\xi^V_{mac} - \xi^I_{mac}$ vs. S_I, i.e. the macroturbulence velocity excess in the I_V data compared to the Stokes I data as a function of the line strength. Symbols are the same as in Fig. 5a

formed in the photosphere, and by Wiehr (1985), who reports amplitudes of 0.1–0.25 km s^{-1} for the Fe I 8468 Å line. These amplitudes are considerably smaller than the values of ξ^V_{mac} we find here, so that we are led to conclude that other mass motions besides the ones induced by the five minute oscillations have to be present in small fluxtubes. However, from the line broadening analysis alone, we cannot differentiate between the effects of a steady flow with a vertical or horizontal velocity gradient, oscillations or waves within single fluxtubes, or steady flows with different flow velocities in different fluxtubes.

By combining the main results of Sects. 3 and 4, we see that motions are present in fluxtubes which strongly broaden the spectral lines, but do not significantly shift them. Oscillations, waves, or a distribution of up- *and* downflows in different fluxtubes (for example via a siphon flow between two fluxtubes connected by a loop) could explain the observations within the context of a (multicomponent) one-dimensional model. Motions outside the fluxtubes may also broaden the Stokes V profiles, even at disk centre, if we take their expanding geometry into account. However, the large difference in ξ^V_{mac} and ξ^I_{mac} (illustrated in Fig. 15) would appear to limit their contribution to the total velocity induced line broadening.

The presence of motions with such large amplitudes means that non-radiative heating may play an important role even in the deep layers of the fluxtube photosphere (cf. Hasan and Schüssler, 1985). They will also have to be taken into account in the empirical modelling of fluxtubes, since their neglect could lead to false values of the empirically determined temperature structure.

Finally, we wish to point out that the present work is exploratory in nature, and contains a number of shortcomings. Firstly the accuracy of the absolute wavelengths of Stokes V can be increased in future FTS observations. This would allow the setting of much stronger constraints on downflow velocities in fluxtubes. The validity of these results can be further checked by looking at the centre to limb variation of the Stokes V wavelengths. First results of such an analysis are presented by Stenflo et al. (1986) who confirm the general absence of sizeable downflows. There is also considerable scope for the improvement of the model calculations. Certainly one of the most drastic simplifying assumptions made is that of one-dimensionality, and calculations with models which take the fluxtube geometry into account will have to be carried out to test the validity of some of the results presented in this paper. In the long term, the data will have to be interpreted in the context of proper physical models of the velocity fields inside and in the immediate surroundings of the fluxtubes. Departures from LTE may affect the shape of the line profiles and thus influence the results.

A problem which has hardly been touched upon in the present paper and which may relate very strongly to the velocity structure of fluxtubes, concerns the mechanism producing the Stokes V asymmetry. We showed in Sect. 4.5 that a strong correlation exists between the amplitude asymmetry of a Stokes V profile and the velocity determined from its width. This result tends to support the notion that the asymmetry of Stokes V is caused, directly or indirectly, by velocity. If strong departures from LTE are present in fluxtubes, then atomic orientation may also give rise to this asymmetry, for example by the mechanism proposed by Landi Degl'Innocenti (1985). Other causes, like simple velocity gradients, or their temporal and spatial combinations, resulting for example from oscillations, are at present at least as viable. The need for, on the one hand, a detailed study of the importance of NLTE effects in fluxtubes using a realistic model atom and, on the other hand, exploratory calculations of the Stokes V asymmetry produced by different velocity fields is therefore acutely felt. Work is in progress on both problems (cf. Solanki and Steenbock, 1986; Pahlke and Solanki, 1986).

Acknowledgments. It is a pleasure to thank J.O. Stenflo for many helpful discussions and for critically reading the manuscript. Å. Nordlund initially suggested part of this work and also provided the continuum opacity code, which is gratefully acknowledged. I am also indebted to H. Wöhl for kindly providing the code for calculating the relative solar-terrestrial velocities, to M. Hayes for fruitful discussions on the transition zone, and to H. Holweger for clarifying comments on the interpretation of macro- and microturbulence. This work was supported by grants No. 2.814-0.83 and 2.666-0.85 from the Swiss National Science Foundation.

References

Athay, R.G., Gurman, J.B., Henze, W., Shine, R.A.: 1982, *Astrophys. J.* **261**, 684
Auer, L.H., Heasley, J.N.: 1978, *Astron. Astrophys.* **64**, 67
Balthasar, H.: 1984, Thesis, University of Göttingen
Balthasar, H., Thiele, U., Wöhl, H.: 1982, *Astron. Astrophys.* **114**, 357
Beckers, J.M.: 1969a, *Solar Phys.* **9**, 372
Beckers, J.M.: 1969b, *Solar Phys.* **10**, 262
Blackwell, D.E., Shallis, M.J.: 1979, *Monthly Notices Roy. Astron. Soc.* **186**, 673
Brault, J.W.: 1978, in G. Godoli, G. Noci, A. Righini (eds.), *Future Solar Optical Observations – Needs and Constraints. Osserv. Mem. Oss. Astrofis. Arcetri* **106**, 33
Caccin, B., Cavallini, F., Ceppatelli, G., Righini, A., Sambuco, A.M.: 1985, *Astron. Astrophys.* **149**, 357
Cavallini, F., Ceppatelli, G., Righini, A.: 1985 *Astron. Astrophys.* **143**, 116

© European Southern Observatory • Provided by the NASA Astrophysics Data System

1986A&A...168..311S

Chapman, G.A.: 1979, *Astrophys. J.* **232**, 923
Crosswhite, H.M.: 1975, *J. Research N.B.S.* **79a**, 17
Defouw, R.J.: 1976, *Astrophys. J.* **209**, 266
Deinzer, W., Hensler, G., Schüssler, M., Weisshaar, E.: 1984, *Astron. Astrophys.* **139**, 435
Dere, K.P., Bartoe, J.-D.F., Brueckner, G.E., Dykton, M.D., Van Hoosier, M.E.: 1981, *Astrophys. J.* **249**, 333
Dravins, D., Larsson, B.: 1984, in S.L. Keil (ed.), *Small-Scale Dynamical Processes in Quiet Stellar Atmospheres*, National Solar Obs., Sacramento Peak, NM, 306
Dravins, D., Larsson, B., Nordlund, Å.: 1986, *Astron. Astrophys.* **158**, 83
Dravins, D., Lindegren, L., Nordlund, Å.: 1981, *Astron. Astrophys.* **96**, 345
Durrant, C.J.: 1977, in E.A. Müller (ed.), *Highlights in Astronomy* **4, II**, 267
Feldman, U., Doschek, G.A.: 1978, *Astron. Astrophys.* **65**, 215
Feldman, U., Cohen, L., Doschek, G.A.: 1982, *Astrophys. J.* **255**, 325
Frazier, E.N.: 1970, *Solar Phys.* **14**, 89
Gabriel A.H.: 1976, *Phil Trans. Roy. Soc. London* **A281**, 339
Gebbie, K.B., Hill, F., Toomre, J., November, L.J., Simon, G.W., Gurman, J.B., Shine, R.A., Woodgate, B.E., Athay, R.G., Bruner, E.C., Rehse, R.A., Tandberg-Hanssen, E.A.: 1981, *Astrophys. J.* **251**, L115
Gingerich, O., Noyes, R.W., Kalkofen, W., Cuny, Y.: 1971, *Solar Phys.* **18**, 347
Giovanelli, R.G., Ramsey, J.V.: 1971, in R. Howard (ed.), *Solar Magnetic Fields, IAU Symp.* **43**, 293
Giovanelli, R.G., Slaughter, C.: 1978, *Solar Phys.* **57**, 255
Giovanelli, R.G., Livingston, W.C., Harvey, J.W.: 1978, *Solar Phys.* **59**, 49
Gustafsson, B.: 1973, *Uppsala Astron. Obs. Ann.* **5**, No. 6
Harvey, J.W.: 1977, in *Highlights of Astronomy*, E.A. Müller (ed.), **4, II**, 223
Hasan, S.S.: 1984, *Astrophys. J.* **285**, 851
Hasan, S.S.: 1985, *Astron. Astrophys.* **143**, 39
Hasan, S.S., Schüssler, M.: 1985, *Astron. Astrophys.* **151**, 69
Hayes, M.: 1985, private communication
Holweger, H.: 1979, in *Proc. XXIInd Liège International Astrophysical Symposium*, Inst. d'Astrophys., Liège, 117
Holweger, H., Gehlsen, M., Ruland, F.: 1978, *Astron. Astrophys.* **70**, 537
Holweger, H., Müller, E.A.: 1974, *Solar Phys.* **39**, 19
Howard, R.: 1971, *Solar Phys.* **16**, 21
Howard, R., Harvey, J.W.: 1970, *Solar Phys.* **12**, 23
Johansson, S.: 1978, *Phys. Scripta* **18**, 217
Jones, H.P.: 1985, in B.W. Lites (ed.), *Chromospheric Diagnostics and Modelling*, National Solar Obs., Sacramento Peak, NM, 175
Kaisig, M., Schröter, E.H.: 1983, *Astron. Astrophys.* **117**, 305
Kemp, J.C., Macek, J.H., Nehring, F.W.: 1984, *Astrophys, J.* **278**, 863
Landi Degl'Innocenti, E.: 1985, in H.U. Schmidt (ed.), *Theoretical Problems in High Resolution Solar Physics*, MPA, Munich, 162
Livingston, W.C.: 1982, *Nature* **297**, 208
Livingston, W.C.: 1983, in J.O. Stenflo (ed.), *Solar and Stellar Magnetic Fields: Origins and Coronal Effects, IAU Symposium* **102**, 149
McWirther, R.W.P., Thonemann, P.C., Wilson, R.: 1975, *Astron. Astrophys.* **40**, 63
Mein, P., Malherbe, J.-M., Schmieder, B., Simon, G., Tandberg-Hanssen, E.: 1985, in B.W. Lites (ed.), *Chromospheric Diagnostics and Modelling*, National Solar Obs., Sacramento Peak, NM, 206
Mihalas, D.: 1978, *Stellar Atmospheres*, Freeman and Company, San Fransisco, pp 279–281
Miller, P., Foukal, P., Keil, S.: 1984, *Solar Phys.* **92**, 33
Moore, C.E.: 1972, *A Multiplet Table of Astrophysical Interest, NSRDS-NBS* **40**
Nordlund Å.: 1978, in A. Reiz and T. Andersen (eds.), *Astronomical Papers dedicated to Bengt Strömgren*, Copenhagen University Observatory, 95
Pahlke, K.D., Solanki, S.K.: 1986, *Mitt. Astron. Gesellschaft* **65**, 162
Pierce A.K., Breckinridge, J.B.: 1973, *KPNO Contr.* **559**
Pneuman, G.W., Solanki, S.K., Stenflo, J.O.: 1986, *Astron. Astrophys.* **154**, 231
Rae, I.C., Roberts, B.: 1982, *Astrophys. J.* **256**, 761
Ribes, E., Rees, D.E., Fang, Ch.: 1985, *Astrophys. J.* **296**, 268
Roberts, B., Webb, A.R.: 1978, *Solar Phys.* **56**, 5
Roberts, B., Webb, A.R.: 1979, *Solar Phys.* **64**, 77
Schüssler, M.: 1984, *Astron. Astrophys.* **140**, 453
Schüssler, M.: 1986, in *Proc. Workshop on Small Magnetic Flux Concentrations in the Solar Photosphere*, Göttingen, Oct. 1–3, 1985, in press
Skumanich, A., Smythe, C., Frazier, E.N.: 1975, *Astrophys. J.* **200**, 747
Smith, M.A., Testerman, L., Evans, J.C.: 1976, *Astrophys. J.* **207**, 308
Solanki, S.K.: 1984, in T.S. Guyenne, J.J. Hunt (eds.), *The Hydromagnetics of the Sun*, ESA **SP–220**, 63
Solanki, S.K.: 1985, in H.U. Schmidt (ed.), *Theoretical Problems in High Resolution Solar Physics*, MPA, Munich, 172
Solanki, S.K., Steenbock, W.: 1986 (in preparation)
Solanki, S.K., Stenflo, J.O.: 1984, *Astron. Astrophys.* **140**, 185
Solanki, S.K., Stenflo, J.O.: 1985, *Astron. Astrophys.* **148**, 123
Solanki, S.K., Stenflo, J.O.: 1986, *Astron. Astrophys.* (in press)
Spruit, H.C.: 1974, *Solar Phys.* **34**, 277
Spruit, H.C.: 1981, *Astron. Astrophys.* **98**, 155
Spruit, H.C., Roberts, B.: 1983, *Nature* **304**, 401
Stenflo, J.O.: 1974, *Solar Phys.* **36**, 495
Stenflo, J.O.: 1976, in V. Bumba and J. Kleczek (eds.), *Basic Mechanisms of Solar Activity, IAU Symp.* **71**, 69
Stenflo J.O.: 1985, *Solar Phys.* **100**, 189
Stenflo J.O., Lindegren, L.: 1977, *Astron. Astrophys.* **59**, 367
Stenflo, J.O., Harvey, J.W.: 1985, *Solar Phys.*, **95**, 99
Stenflo, J.O., Harvey, J.W., Brault, J.W., Solanki, S.K.: 1984, *Astron. Astrophys.* **131**, 33
Stenflo, J.O., Solanki, S.K., Harvey, J.W.: 1986, *Astron. Astrophys.* (in press)
Unno, W., Ribes, E.: 1979, *Astron. Astrophys.* **73**, 314
Unsöld, A.: 1955, *Physik der Sternatmosphären*, 2nd. Ed., Springer Verlag, Berlin
Van Ballegooijen, A.A.: 1985 in M.J. Hagyard (ed.), *Measurements of solar Vector Magnetic Fields, NASA Conf. Publ.* **2374**, 322
Wiehr, E.: 1985, *Astron. Astrophys.* **149**, 217

© European Southern Observatory • Provided by the NASA Astrophysics Data System